Sasol Advanced Fuels Laboratory

UNIVERSITY OF CAPE TOWN

An evaluation of the use of thermocouples for gas temperature determination in an I.C engine environment

Author:

Ngonidzashe G. Kundhlande

Supervised by:

Prof. Andy Yates

A dissertation submitted to the Department of Mechanical Engineering, University of Cape Town, in partial fulfilment of the requirements for the degree of Master of Science in Engineering

Cape Town, South Africa
27 March 2007

Declaration

1. I know that plagiarism is wrong. Plagiarism is to use another's work and pretend that it is one's own.

2. I have used the Harvard convention for citation and referencing. Each significant contribution to, and quotation in this project from the works of other people has been attributed, and has been cited and referenced.

3. This project is my own work.

4. I have not allowed, and will not allow anyone to copy my work with the intention of passing it off as his or her own work.

Signature Signed by candidate

Date 27/03/2007

Acknowledgements

Firstly I would like to thank the Lord for granting me the wisdom, strength and good health that I enjoyed throughout the duration of this project.

I would like to extend my most sincere gratitude to my supervisor, Prof. Andy Yates, for his insightful suggestions and guidance throughout the course of this project.

I would like to thank Sasol for funding this project.

I would also like to thank Kim Cloete for fabricating the thermocouple probes used in this project.

Lastly I would like to thank my family and friends for their support and prayers, may God bless them all.

Abstract

The magnitude and transient nature of the gas temperature in the cylinder of an internal combustion engine makes the measurement quite difficult. Several techniques have been employed to try and determine the actual gas temperatures in internal combustion engines, and most of these have either shown inconsistency or turned out to be extremely expensive.

In this thesis, the use of a thermocouple to determine the gas temperature was explored. It was known from the outset that the thermal inertia would not allow the thermocouple to track the gas temperature. However, at some point during the rise and fall of the gas temperature, a state of thermal equilibrium would be achieved between the thermocouple and the surrounding gas. At this postulated equilibrium point, the thermocouple temperature would be constant and the gas temperature would be inferred at this instant. The gas temperature for the rest of the cycle would then be calculated from this point. For the fired engine cycles it would be necessary for the minimum thermocouple temperature to occur during the compression stroke before the spark event, while conditions are still considered to be homogeneous.

A mathematical model was set up to predict the engine breathing, compression, and fuel combustion. A heat transfer model for the thermocouple was also set up to optimise the appropriate physical parameters (i.e. length and diameter) of the thermocouple. Tests were conducted on a CFR engine to evaluate the validity of the concept and the initial model. After initial tests, the method and the model both appeared to be satisfactory, and other thermocouple probes were designed based on this model.

At the second stage of the project, two unsheathed thermocouple probes with a wire diameter of 0.2mm were designed to protrude 2mm and 4mm into the cylinder of the engine. Tests were conducted on the CFR engine while being motored and fired, and at different engine speeds, compression ratio, and equivalence ratio for the fired engine. Results for the 4mm thermocouple were deemed not useful since the results from the fired engine all had the minimum thermocouple temperature occurring after the spark ignition had occurred.

It was found that the initial numerical model was inadequate to describe the temperature for the 2mm and the 4mm thermocouple probes, so a boundary layer model to estimate the temperature profile within the cylinder had to be considered. The boundary layer model was added to the already existing numerical model. The revised numerical model managed to describe the temperature in the 2mm thermocouple with acceptable accuracy, but was inadequate in describing the temperature for the 4mm probe. This was because the formulation

used to model the velocity profile within the boundary layer described by Foster and Witze (1987), was inconsistent with the velocity profile modelled for the CFR engine by Hsiao (2006).

From the modelled results an equation that compensated for boundary layer thickness and conduction to the wall temperature was developed. This modification managed to reproduce gas temperature for the motored engine to an accuracy of about ±40°C, at the CAD of calculation, when compared to temperatures estimated using an ideal gas calculation. An attempt to apply the same equation to the fired engine tests was not successful and under-estimated the gas temperature by as much as 100°C at the CAD of calculation, when compared to temperature values estimated from a simulation of the measured pressure.

Upon evaluating the findings of this project, and reviewing the literature available, it was recommended that the use of acoustic methods of measuring the gas temperature would be a more viable alternative. This was motivated by their well published relative simplicity and inexpensiveness as compared to alternative laser based methods.

Table of Contents

Appendices

List of Figures

List of Tables

Nomenclature

α	-	Thermal diffusivity
γ	-	C_p/C_v for air
δ	-	Boundary layer thickness
θ	-	Current crank angle
λ	-	1/equivalence ratio
μ	-	Dynamic viscosity
ρ	-	Density
c	-	Sonic velocity
k	-	Thermal conductivity
h	-	Convection heat transfer coefficient
m	-	Mass
t	-	Time
v	-	Velocity
x	-	Distance from wall
x_b	-	mass fraction burned
A	-	Area
C_d	-	discharge coefficient
C_p, C_v	-	specific heat capacity
CR	-	compression ratio
D	-	Diameter
F	-	Frictional coefficient
K	-	Entry loss coefficient
L	-	Length
N	-	Engine speed
P	-	Pressure
R	-	Specific gas constant
T	-	Temperature
V	-	Volume
Nu	-	Nusselt Number
Re	-	Reynolds' Number
Pr	-	Prandlt Number
BDC	-	Bottom Dead Centre

CAD	-	Crank Angle Degrees
CFD	-	Computational Fluid Dynamics
CFR	-	Cooperative Fuel Research
EVC	-	Exhaust Valve Close
EVO	-	Exhaust Valve Open
HCCI	-	Homogeneous Charge Compression Ignition
IVO	-	Inlet Valve Open
IVC	-	Inlet Valve Close
TDC	-	Top Dead Centre

1. Introduction

1.1 Project background

Gas temperature measurement in the combustion chamber is a significant aspect of the study and development of internal combustion engines. Gas temperatures are important in determining the engine efficiencies, in the formation of exhaust emissions, and in fuels research. One of the main benefits of being able to measure gas temperature in a combustion engine accurately is to enable researchers to validate computer models used in the prediction of the combustion process.

However the transient nature and the absolute magnitude of the gas temperature in the cylinder of the internal combustion engine makes the measurement difficult. Over the years, several techniques have been employed to try and determine the actual in-cylinder gas temperatures. These techniques include direct measurement by means of a thermocouple, acoustics, and laser-based techniques where the gas temperature would then be inferred, but they have either shown inconsistency or turned out to be impractical or too expensive.

The research group at the Sasol Advanced Fuels Laboratory needed an inexpensive and robust technique to measure the gas temperature in an engine. The method proposed in this thesis involves using a thermocouple to deduce the gas temperature at one instant during the compression stroke.

1.2 Project objectives

The purpose of this project was to investigate the possibilities of making use of the thermocouple probe to determine the gas temperature at one instant inside the cylinder of an internal combustion engine. This was to be done in the region of the combustion chamber where the thermocouple temperature would not exceed the metallurgical limit of the probe, and inferring the gas temperature from the reading given by the thermocouple.

- A mathematical model was used to characterise the physical parameters of this probe.
- An experimental thermocouple probe was built to ascertain the accuracy and the precision of this model.
- Deficiencies in numerical model were identified and the model was reworked to improve the correlation between the measured and predicted thermocouple temperature under motoring conditions.
- The measured thermocouple data was used to predict the in-cylinder gas temperature.

1.3 Proposed hypothesis

The following method was proposed at the onset of this project as a potential solution.

- Create an engine combustion and heat transfer numerical model to predict the gas temperatures inside the engine, and determine the plausibility of the method and the physical parameters of the thermocouple.
- The proposed thermocouple would have to able to track the gas temperature on a diminished scale in such a way that the thermocouple temperature would be in decline during exhaust and inlet strokes, as the gas temperature starts to rise during compression, an upswing in the thermocouple temperature would occur. The thermocouple temperature at which this upturn would occur would represent an equilibrium point where the thermocouple temperature and the gas temperature would be assumed to be equal. From this assumed equilibrium temperature, the gas temperature for the rest of the cycle would be calculated using measured pressure data. Temperatures would then also be calculated back to inlet valve closure conditions.
- For the fired engine, the equilibrium point would have to occur before the spark occurred. This is because after the spark has occurred and the flame is propagating through the cylinder, the conditions in the cylinder are no longer homogeneous.
- It would be possibly necessary to have the hot junction of the thermocouple as close to the wall as possible and to have strong thermal contact with the wall, so as to be able to conduct heat to the wall at high temperatures. This is to prevent the thermocouple from burning during combustion.
- Ideally have the thermocouple thin enough so as to obtain a temperature swing with sufficient magnitude to enable adequate experimental resolution of the equilibrium point.
- With the thermocouple inserted into the combustion chamber, measurements would be taken and compared against initial modelling results. The model would then be reworked to match the actual result. This would be used to calibrate the model for future use.

1.4 Layout of document

This document is structured as follows:

The following chapter explores literature relevant to this project, focusing on methods used to measure gas temperature in engines, the use of thermocouples in temperature measurement, engine modelling, and heat transfer in engines.

Chapter 3 follows with the theoretical development of the project, how the engine combustion and boundary layer models were set up, and the reasoning behind the heat transfer model used in the project.

Chapter 4 explains how the thermocouples used in the experiment were built and the tests that were run on the CFR engine.

In Chapter 5 and Chapter 6 the test results and the results from the modelling work are presented and analysed. This is done with the view of assessing the effectiveness of the method and the validity of the model.

Based on the results, conclusions and recommendations for future work will follow. The appendices show the details of the models used in the investigation.

2. Literature Review

The measurement of gas temperature and wall temperature of internal combustion engines and the heat flux to the walls of the cylinder has been explored by many researchers. It was important and relevant for this project to review previous work done in measuring gas and wall temperature. A review of the previous use of thermocouples in measuring temperature in a transient situation, and understanding their limitations is also described in this section. Because of its particular relevance to this project, heat transfer in internal combustion engines and conventional heat transfer theories were also reviewed.

2.1 Gas temperature measurement in an Internal Combustion Engine

Measurement of in-cylinder gas temperatures has been an ongoing subject of research in the field of automotive development. In-cylinder gas temperatures have an effect on the volumetric efficiency, knock, and NO_x formation. Exhaust gas temperatures also affect the oxidation of hydrocarbons in the exhaust thereby indirectly affecting emissions. Several methods have been developed for measuring gas temperatures in the cylinders of internal combustion engines. Several optical techniques have been developed in attempts to measure temperature non-intrusively along with acoustic methods, most of which have only been successful to a limited extent.

2.1.1 Coherent Anti-Stokes Raman Spectroscopy

Coherent Anti-Stokes Raman Spectroscopy (CARS) is a well developed technique for temperature measurement, and has been used to measure temperature non-intrusively in internal combustion engines. The CARS technique probes the population distribution of molecular energy rotational energy levels, which can be used to calculate the temperature. CARS can be used to measure the temperature of nitrogen and oxygen or mixtures of the two (Bood et al, 1997). The CARS technique can also provide temperature measurements with a spatial resolution of 50μm (Lucht et al, 1991).

Transient end gas temperature measurement has been done by Bood et al (1997) in a modified single cylinder engine, where the end gas pocket was produced in a desired location in the cylinder. Bood et al wanted to measure the temperature of the end gas before the onset of knocking. Measurements done during the compression of the end gas corresponded with the calculated values. Single shot measurements done at -42CAD showed a standard deviation of about 2.5% from the mean due to the statistical laser mode fluctuations inherent in the measuring technique. This error could amount to about 25K at some locations. Measurements

done by Lucht et al (1991) in the thermal boundary layer of an engine using the CARS method show a scatter of about 10-20K in the core gas.

2.1.2 Emission Absorption Spectroscopy

Emission-absorption has also been used to infer the temperature in internal combustion engines. Aust et al (1999) used emission-absorption spectroscopy to measure crank angle resolved temperatures in the combustion chamber of a standard production engine. The technique involved the use of a chopped laser beam through the combustion chamber via specially designed optical sensor assemblies. This method involves simultaneous measurement of the spectral radiance and spectral absorptance along the line of sight. Both the radiance and absorptance are dependant on the wavelength, temperature and the species present in the combustion chamber. In non-equilibrium conditions the measured data would give an 'excitation temperature' which could be around 300K above the actual temperature. With the gas seeded with potassium, equilibrium temperatures could be measured, and it was assumed that the amounts of potassium added to the gas had a negligible effect on the combustion process. Potassium is in thermal equilibrium during combustion and as only atomic potassium is formed in the burnt zone, actual burnt zone temperatures could be derived.

Visible spectral emission and spectral absorption signals were recorded alternately with 1° crank angle resolution yielding combustion temperatures according to Planck's and Kirchhoff's radiation laws.

For steady state conditions, comparisons were made for temperatures derived using a two-zone thermodynamic model from the pressure readings and temperatures derived from the spectroscopic method, but this method was not applicable for transient or cold start temperature measurement, so only the spectroscopic method was used for these cases. The pressure data measured was of sufficient accuracy but the temperature accuracy was restricted by certain assumptions.

Temperature from the thermodynamic model agreed well with the temperature for the spectral method to within about 50K. Deviation from the two methods at times arose because of the fact that the thermodynamic analysis represented average temperatures of the whole combustion volume, whereas the spectral method averages the temperature along the line of sight. It was concluded that the accuracy of the spectroscopic method was of the order of 50K.

2.1.3 Fiber Optic Heterodyne Interferometry

A fiber optical heterodyne interferometry system has been developed to measure high resolution temperature histories for unburned and burned gases in combustion chambers non-intrusively. This method was found to be fairly insensitive to fluctuations caused by mechanical vibrations. Gas temperatures were measured during the compression stroke of the engine (Kawahara et al, 2001).

The system's principles are shown in Figure 2-1. Since the refractive index is affected by the temperature and gas species concentrations, the gas composition is required to calculate the temperature.

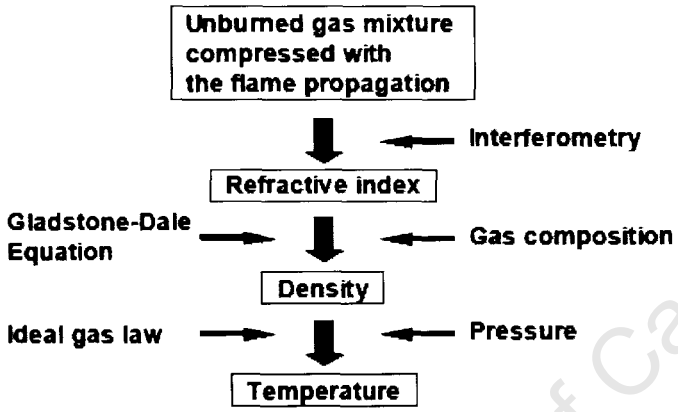

Figure 2-1: Principle of temperature measurement using laser interferometry (Kawahara et al, 2001)

For the temperature calculation it is necessary that the initial pressure and temperature be known, and then the temperature would be calculated from the pressure and the change in frequency.

Kawahara et al did tests in a constant volume vessel where propane-air or methane-air mixtures were used. The inlet pressure and temperature were measured using a mercury manometer and a J-type thermocouple respectively. A reference signal was kept out of the combustion chamber while the test signal was passed through the combustion chamber and the phase shift in the waves was calculated from the resulting difference in frequency beats. It was shown that the temperature of the unburned gas as measured by the heterodyne was almost equal to that calculated assuming adiabatic compression of the gas, thus it was assumed that the compression process was adiabatic for the duration of flame propagation.

Kawahara et al also did tests during the compression stroke of an engine. A homogeneous fuel/air mixture was stored in a separate tank and inducted into the engine via a pipe through a valve at the centre of the cylinder axis, so the mixture was inducted with no swirl. Compression

of the gas started at BDC and the initial gas temperature at inlet valve closure was measured by a resistance wire thermometer, and then calculated using the pressure and the heterodyne signal. The result of this technique correlated with the temperature calculated assuming the polytropic compression of air, where the temperature at IVC was measured using a resistance wire as a thermometer.

2.1.4 Acoustic Thermometry

Acoustic techniques of measuring gas temperature are attractive because of the relative simplicity and are relatively inexpensive compared to the specialised laser techniques. The technique also has a potentially faster response compared to thermocouples. The basic procedure for this technique is as follows: two transducers are placed across the intended medium at a known distance apart. A signal is sent across this medium and the time of flight is recorded. The velocity of the sound through a gas is a function of the temperature and composition so, given a known composition, the temperature can be calculated. The average temperature is inferred from Equation 2-1. In the case of internal combustion engines, during the experiment the fuel/air ratio is measured in the exhaust and is used to estimate the gas composition in the cylinder, uncertainties are introduced by the residual gas mass, which is unknown (Bauer et al, 1997).

Equation 2-1

$$c = \sqrt{\gamma RT}$$

In work done by Bauer et al (1997) on a single cylinder Ricardo MK III engine crankcase fitted with a Volvo 4 valve cylinder head, the two transducers were inserted into holes facing each other across the cylinder. When firing the engine, results were obtained during the compression part and the early expansion of the engine cycle, low pressure and high temperature conditions in the later part of the cycle were detrimental to receiving a signal. In the simulation, the ideal gas law was used, using the mass calculated from the temperature derived from the sonic velocity of gas and the measured pressure.

During measurement losses occur, which lead to difficulties in signal processing. Transmission losses and attenuation loses are suffered through the whole process, and these are dependant on temperature and pressure. In the cylinder the pressure and temperature vary widely thus causing different conditions for signal processing.

Uncertainties in the measurement also stem from time of flight detection, with the main issue being the clear identification of the start of sound transmission and the detectors' response to the signal. The time when a signal is sent to the sound transducer to the time when a

noticeable sound signal is emitted and received is difficult to determine with precision. The uncertainty introduced by this is illustrated in Figure 2-2, where a comparison of the simulated actual scheme to the ideal situation is shown. Uncertainties in the measurement also stem from gas composition uncertainties and gas temperature distribution. These uncertainties are much larger in the burnt region and result in an aggregate uncertainty of about 125K.

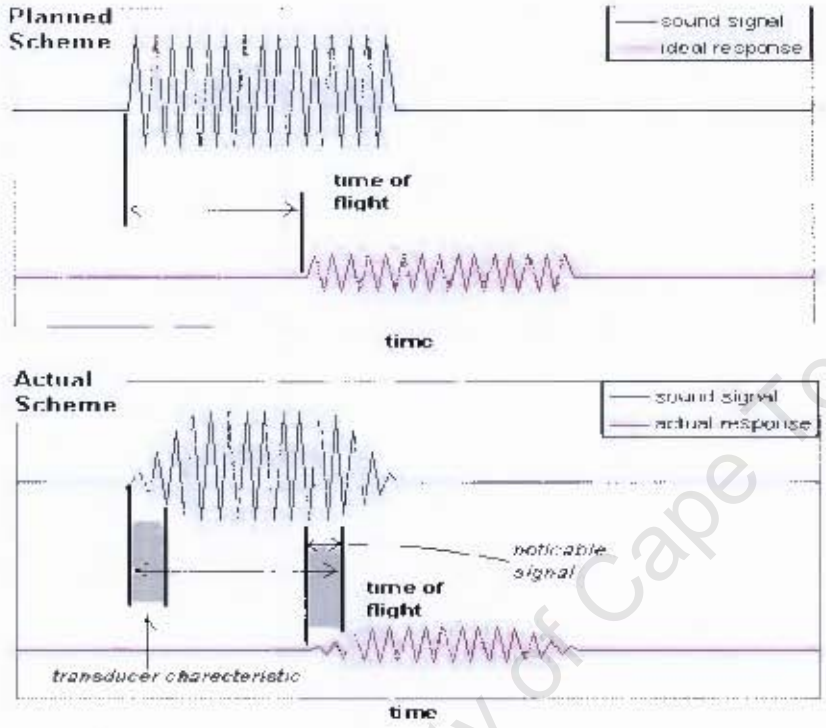

Figure 2-2: Figure showing the uncertainty introduced by transmitter and receiver characteristics

2.1.5 Wavelength-Agile Absorption Spectroscopy

In-cylinder gas temperature measurements have been carried out in an HCCI engine using a wavelength-agile absorption sensor with a fiber coupled LED. The gas temperature was inferred from the H_2O absorption features. The absorbance spectra measured from the engine at a particular crank angle degree is integrated and compared to a synthetic library of absorbance features at the measured pressure and similar H_2O mole fraction. Research was done to get a better understanding of the operation of the HCCI engine by measuring the temperature during compression and ignition of the engine. Measurements were done on a single cylinder engine which allowed for lubricant-free operation and optical access to the cylinder volume via opposed quartz windows (Sanders et al. 2003).

Sanders et al conducted their measurements while the engine was being motored and with two lean fuel/air mixtures. Measurements were compared with mass average calculated gas temperatures and isentropic calculations and they showed an accuracy estimated to be ±30K.

Comment: *On consideration of the techniques reviewed, all the techniques reported similar accuracies. Although the CARS method is able to provide spatial variations in temperature, the other methods which measure the temperature along the line of sight, are sufficient in validating models where an average gas temperature is adequate. In such situations the acoustic technique of measuring temperature is viable because of its simplicity and inexpensiveness when compared to the specialised laser techniques, and is shown not to compromise accuracy too severely in comparison to other techniques.*

2.2 Temperature measurement using thermocouples

When measuring temperature in a flowing fluid environment, the sensor has to be in thermal contact with the fluid being measured. When there is no heat transfer the system is said to be in thermal equilibrium and the sensor temperature and gas temperature are equal. In reality, if the sensor is immersed in the medium it is measuring, the sensor temperature and the gas temperature will not be perfectly equal because of conduction along the length of the sensor to or from the wall of the vessel where it is thermally connected (Cessac, 2003).

2.2.1 Heat Flux probes

Thermocouples are used for heat flux measurements in industrial applications. Thin film thermocouple sensors are usually used to obtain transient temperature measurements for different operations. Fast response from thermocouples is achieved when a thin junction is formed between the two thermocouple metals. Ishii et al (2000) measured the transient wall temperature in an internal combustion engine successfully using thin film thermocouples, and then conducted numerical analysis on the acquired values. Sanderson and Sturtevant (2002) mention that one way to create a thin film sensor is to use abrasion on the exposed part of the sensor to create a burr across the small gap. This guarantees a thin junction, although the method involves very fine tolerances.

2.2.2 Flowing gas temperature measurement

Measurement of gas temperature in a flowing environment using thermocouples where fast response and the effect of the surrounding environment has to be minimal, has been undertaken by Enomoto et al (1997). Enomoto et al were trying to measure the temperature of the input charge of an internal combustion engine using ultra thin thermocouples mounted in the inlet gas stream at the inlet valve, just in front of the combustion chamber, as shown in Figure 2-3.

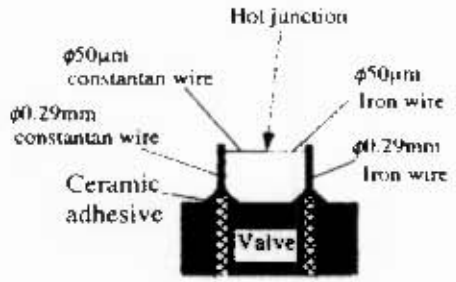

Figure 2-3: Figure showing the ultra thin thermocouple used to measure intake gas temperatures

This particular method was used in an attempt to negate the effect of heat conduction from the valve to the thermocouple, and the heat capacity of the thermocouple. However, it was realised that the sensor still had a time constant of about 21-29ms due to the thermo-physical properties of the thermocouple and the intake gas.

Thermocouples have also been used to measure an instantaneous gas temperature in the exhaust stream of a spark ignition engine. Kar et al (2004) developed a compensation technique to estimate a time constant to account for the slow dynamic response of the thermocouple, and thus reconstruct the transient temperature being measured. This technique was developed with limited success by Kar et al, showing a difference of only 30K on compared results. In principle, this is not far removed from the hypothesis underlying the present research, however the method used by Kar et al would not be applicable to this project as it was assumed that conduction heat transfer was negligible.

2.2.3 Measuring the wall temperature of an Internal Combustion Engine

A method of measuring the wall temperature by imbedding a thermocouple within the wall of the engine and keeping the hot junction as close to the surface as possible was also devised by Enomoto et al. Figure 2-4 shows how these junctions were created. This method was successful in measuring wall temperatures and Enomoto et al noticed that the wall temperature did not vary greatly during the engine cycle, so a constant value for wall temperature was assumed.

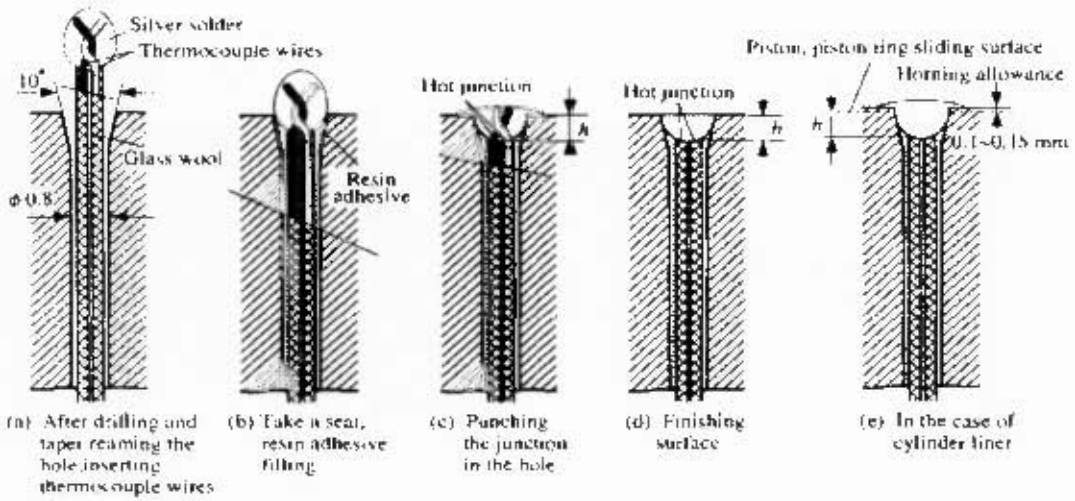

Figure 2-4: Figure showing how thermocouples embedded in the wall of an engine are created

Comment: *The use of thermocouples is a simple and well understood way of measuring temperatures. However, measurement of transient temperatures using thermocouples has been shown to lag, due to the physical properties of the probe, and this is expected to persist in this project. However the lack of literature regarding the proposed method for this project left an opportunity for investigation. Since the proposed technique only captures the temperature at one instant during the cycle, a model to simulate the rest of the cycle has to be created.*

2.3 Engine modelling

2.3.1 Combustion cycle modelling

Combustion models have been developed by many researchers and have been used to predict the conditions within the cylinder of an internal combustion engine. The combustion models make use of general thermodynamic principles to calculate the pressure and temperature at the corresponding CAD. Models are usually based on the first law of thermodynamics, and the conservation of mass, while maintaining chemical equilibrium of all the species involved. Continuous development of combustion models has led to different types of models being developed. These range from the very simple single zone models where combustion is assumed to be instantaneous and all combustion reactants are consumed at the start of combustion to two-zone models and three-zone models where combustion takes a finite time to occur.

Two-zone models which describe the combustion process more realistically than the single zone model are a more common descriptor for engine research applications. In this type of model the cylinder volume is separated into two zones, the unburned zone which contains the reactants and the burned zone which contains the combustion products. In this type of model the flame is assumed to propagate from the spark creating a burned region that grows from the

spark towards the rest of the cylinder as shown in Figure 2-5. In this type of model the combustion efficiency is often assumed to be 100%, and the mass fraction burned is described by an empirically determined descriptor.

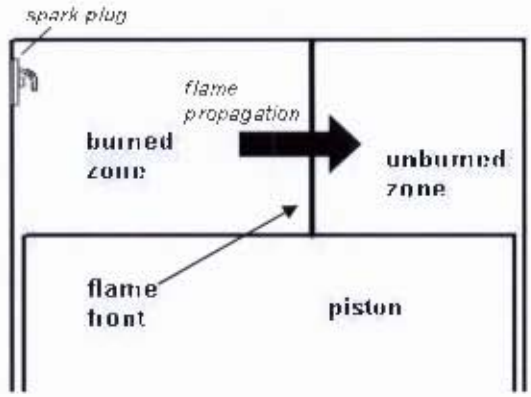

Figure 2-5: Simple two zone model showing flame front propagating toward the wall

The rate at which the fuel/air mixture burns increases from a low value immediately after the spark to a maximum value approximately halfway through the burn duration then reduces to zero at the end of the combustion process. The burn duration can be described in two almost distinct phases; the flame development phase and the rapid burn phase, this is shown in Figure 2-6. The flame development angle is described as the period after spark is discharged until significant cylinder mass has been burned, this is typically between 5-10%. The rapid burn angle is the period where the bulk of the charge burns, from the flame development stage to the end of the combustion process (Heywood, 1988). In this formulation a mass and energy balance is maintained between the unburned and burned zones.

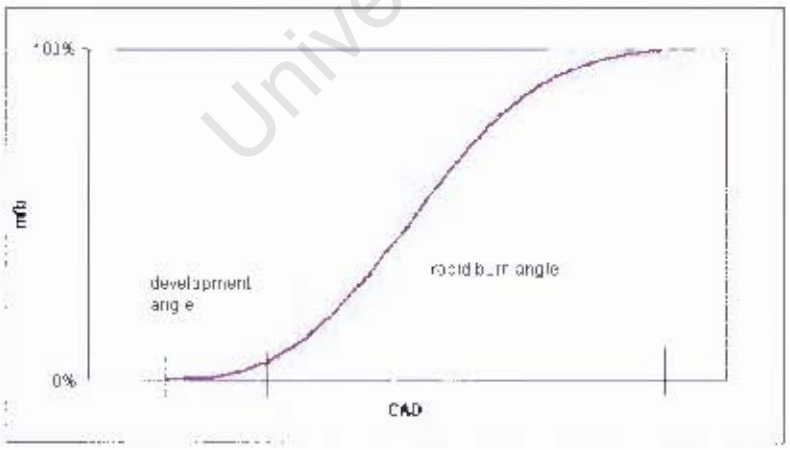

Figure 2-6: Curve describing the flame development angle and rapid burn angle versus crank angle degree

Three-zone models describe processes in an engine in more detail than the other types of modelling. They consist of an unburned region, a burned region and a boundary layer region close to the cylinder walls where combustion does not take place completely. The thermal boundary layer is believed to be responsible for the formation of hydrocarbon emissions from

the engine because it quenches the flame as it approaches the cylinder walls. Work done by Fiveland and Assanis (2001) predict that for certain cases as much as 15% of fuel mass may be potentially quenched by the boundary layer. A simple model of this is shown in Figure 2-7.

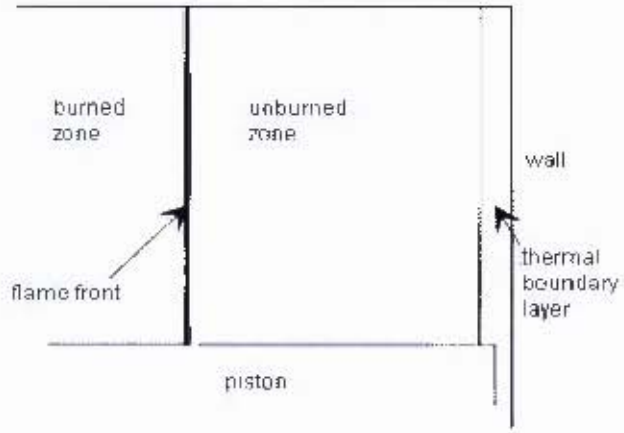

Figure 2-7: A simplified three zone model, showing a vertical flame front propagating towards the wall

2.4 Boundary layer modelling

Several models have been developed to predict heat flux using conventional boundary layer theory, and there has been a clear indication that gas motion and pressure change are the dominant parameters which influence the boundary layer temperature distribution.

Research shows that there are isotherms parallel to the cylinder wall, but this profile is distorted at the piston/cylinder wall and cylinder wall/head intersections. Therefore, in modelling the thermal boundary layer, the cylinder is generally separated into different sub-modes and the geometric centres are represented by nodes, where the temperature, density, composition and other properties are assumed to be constant within that mass (Jenkin et al, 1996a). Figure 2-8 depicts this method.

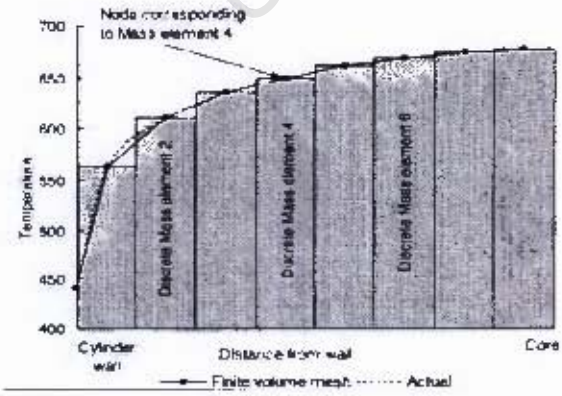

Figure 2-8: Mass inside a cylinder is broken into discrete masses (Jenkin et al, 1996a)

Figure 2-9 shows the profile in the velocity and thermal boundary layers. It is apparent from the picture that the thermal boundary layer extends beyond the influence of the velocity boundary

layer. Between the outer "constant" eddy conductivity region and the near wall laminar region is a transition region roughly corresponding to the overlap of the velocity and thermal boundary layers (Jenkin et al, 1996a), (Foster and Witze, 1987).

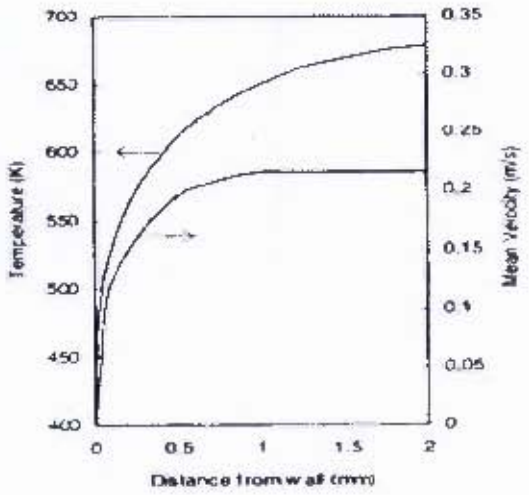

Figure 2-9: The temperature profile and the velocity profile in the boundary layer (Jenkin et al, 1996a)

2.4.1 Thermal boundary layer

A thermal boundary is known to exist at the walls of internal combustion engines. Research has shown that the thermal boundary layer affects the heat transfer to the walls of the engine (Jenkin et al, 1996b). Measurements have been done to determine the effect of boundary layers on the heat transfer by Lucht et al (1991). These effects have been modelled by Jenkin et al (1996b) and Lawton (1987) and have shown that heat transfer in the engine is closely related to the boundary layer profile.

The thickness of the thermal boundary layer has been measured by Lyford-Pike and Heywood (1984) and the results are illustrated in Figure 2-10. They found that the boundary layer thickness decreases during the intake stroke, and increases steadily during compression and expansion. it then stops growing and becomes unstable during the exhaust process, separating from the wall and interacting with the bulk gas leaving the chamber.

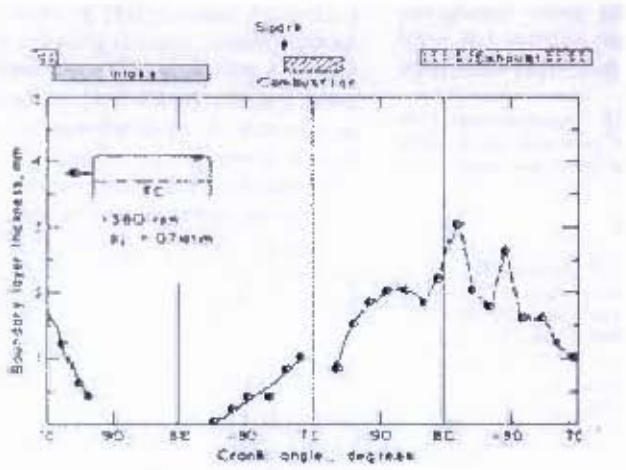

Figure 2-10: Thermal boundary layer thickness measured in the clearance volume

2.4.2 Velocity boundary layer

Velocity measurements in a cylinder have been carried out and it has been established that a momentum boundary layer exists on the walls. "However, there is good evidence to suggest that conventional, fully developed turbulent boundary layer theory is not applicable to engine type flows primarily due to the high turbulence intensities in the "free stream" core bulk flow" (Jenkin et al, 1996a, page 5).

Research by Foster and Witze (1987) shows that the velocity profile in the boundary layer in a low swirl and high swirl internal combustion can be approximated by the Blasius boundary layer function and the seventh power law which is generally used in turbulent boundary layers.

It has also been shown that the velocity boundary layer is much smaller than the thermal boundary layer and the thickness of the velocity boundary layer is generally proportional to the thickness of the thermal boundary layer. This proportionality is governed by the Prandlt number of the flowing fluid (Arpaci and Larsen, 1984).

Comment: *For the requirements of this project a two-zone model would be sufficient to describe the engine cycle. Although the three-zone model is said to be more accurate than the two-zone model, it was not necessary for this project to estimate the hydrocarbons in the boundary layer. It was however necessary for this project to be able to estimate a temperature profile and a velocity profile in the boundary layer for the heat transfer calculation.*

2.5 Heat transfer in SI engines

Heat transfer in internal combustion engines has been the subject of several previous studies. Though there have been many measurements of heat flux in internal combustion engines,

Annand and Woschni published formulas for estimating the heat transfer, which are widely used.

2.5.1 Heat transfer in the cylinder of a SI engine

Annand's and Woschni's formulation of estimating convective heat transfer from the gas to the walls of internal combustion engines are the most commonly used when predicting heat transfer. These formulations are averaged over the volume of the cylinder, and the heat transfer coefficients and other gas properties are calculated at average gas cylinder temperature.

The Nusselt number for both formulations is formulated for varying engine designs and charge motion (Heywood, 1988).

Annand and Woschni produced quasi-steady state heat transfer equations and ignored the non steady effects produced by the boundary layer. However research has shown that heat transfer is at times in the opposite direction as to what logic would suggest due to boundary layer effects (Lawton, 1987).

2.5.2 Heat transfer during charge induction

The intake process is characterised by three distinct flow phases: overlap backflow, which occurs when cylinder pressure is higher than intake manifold pressure at the end of expansion; forward flow, which occurs when the piston is moving downwards drawing air into the cylinder; and displacement backflow, when the intake valve is still open and the piston is pushing the air out, which occurs mainly at low speeds.

Work has been done to determine the heat transfer in the intake manifold of a spark ignition engine by Bauer et al (1996). The work involved single cylinder engines with similar geometries; where in one engine the intake gas temperature was measured using a fast response thin wire resistance thermometer placed at five locations along the manifold, and these were compared to CFD calculations done for the engine. It is argued that while the engines are different, the similarities served the purpose of a more qualitative understanding.

Results shown in Figure 2-11 show the presence of residual burnt gas soon after overlap backflow, and Figure 2-12 shows that close to the cylinder there is a rise in gas temperature in the intake manifold due heat transfer to the gas from the engine walls. Figure 2-12 suggests that the gas which is displaced into the intake manifold towards the end of the intake stroke is much hotter than the ambient temperature.

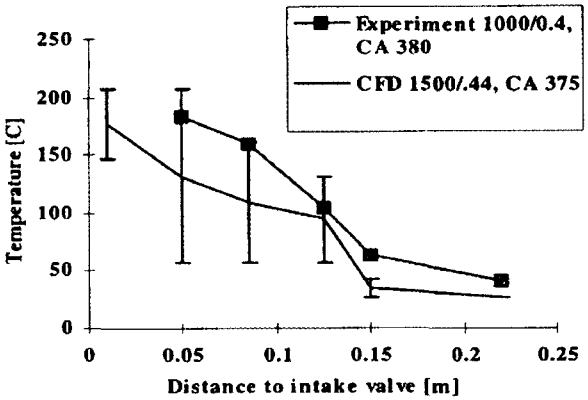

Figure 2-11: End of valve overlap backflow, comparison of experimental and predicted gas temperatures.

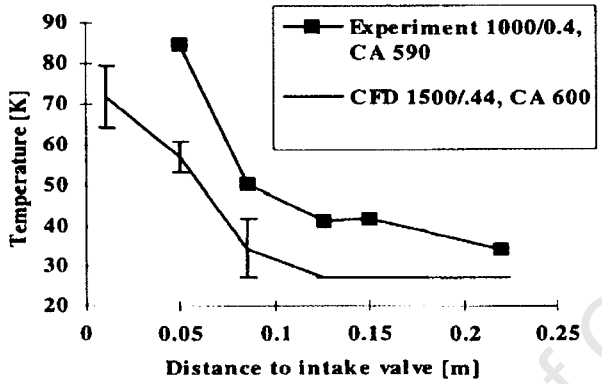

Figure 2-12: End of displacement backflow, comparison of experimental and predicted gas temperatures.

Figure 2-13 shows the temperature in the inlet manifold during the forward flow. There is a temperature rise as the gas approaches the cylinder, which might be due to the presence of residual gas or heat transfer. These effects were separated by raising the inlet gas temperature to the wall temperature thus reducing heat transfer. The effect of this is shown in Figure 2-14. There is still a temperature rise in the gas, which is probably due to the continuing presence of burnt residual gas.

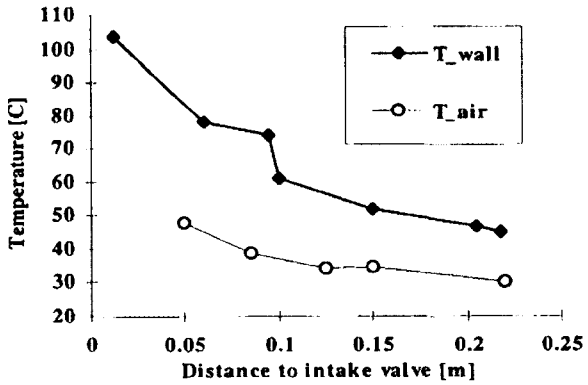

Figure 2-13: Experiment using ambient air as charge gas, forward flow CA 530, fresh gas temperature 30° C, coolant temperature 75° C, 1500 rpm / 0.6 bar.

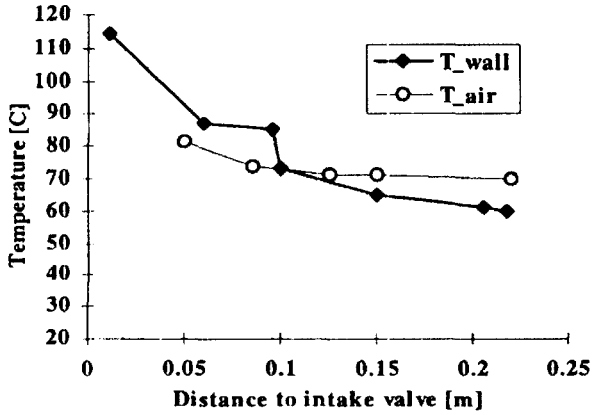

Figure 2-14: Experiment using preheated air as charge gas, forward flow 530° CA, fresh gas temperature 70° C, coolant temperature 75° C, 1500 rpm/0.6 bar.

The gas temperature measurements confirmed the penetration depth of the residual gas backflow of about 15cm, obtained from the CFD and the experiment. The rise of the inlet gas temperature in the manifold even when the initial temperature was raised showed the continuing presence of the burnt gas during forward flow.

The paper by Bauer et al did not seem to account for any radiation heat transfer from the manifold walls and the inlet valve. The possibility of the temperature of the thermocouple rising due to the stagnation of air on the thermocouple probe has also been ignored. The conversion of kinetic energy to heat energy at an assumed static temperature of 300K and inlet gas velocities of 300m/s gives rise to temperature increases of approximately 45K. This could have been significant in the measurements.

3. Theoretical Development

It was of paramount importance to this project to be able to numerically model the complete engine cycle and heat transfer to and from the thermocouple, both for the purposes of initial design and verification of the method. This section contains the basic formulation of a complete engine cycle model, including a boundary layer model since it was found that the thermocouple was mostly in the boundary layer, and the heat transfer model used to predict the temperature of the thermocouple during the full engine cycle.

3.1 Engine modelling

The mainstay of this project was centred on the ability to empirically and mathematically reproduce the pressure traces measured from the engine using a simple model. Although this was possible to a certain extent, the model had several known drawbacks because of some assumptions used to idealise the formulation for the purposes of simple computation.

3.1.1 Combustion thermodynamics and chemistry

In an ideal four stroke spark ignition engine the fuel/air mixture is compressed by the piston to a higher temperature and pressure. The mixture is then ignited by a spark and the combustion causes the pressure and temperature to rise and force the piston downwards. The combustion products leave the cylinder and fresh charge is inducted for the start of another cycle. An overall energy balance is maintained in the cylinder according to the first law of thermodynamics.

Equation 3-1

$$\Delta Q - \Delta W = \Delta U$$

An ideal complete combustion of general hydrocarbon fuel with air under stoichiometric conditions is shown in Equation 3-2.

Equation 3-2

$$C_x H_y + \left(x + \frac{y}{4}\right)(O_2 + 3.773N_2) \rightarrow xCO_2 + \frac{y}{2}H_2O + 3.773\left(x + \frac{y}{4}\right)N_2$$

The nitrogen in the air is assumed to be inert during the reaction, because when products are at low temperatures it is not affected by the reaction. (Heywood 1988)

Due to the high in pressure and temperature in the cylinder some equilibrium reactions will take place, namely CO2 dissociation and the water gas shift reaction which gives rise to the

formation of CO and H2 within the products of the reaction. This is shown in Equation 3-3 and Equation 3-4.

Equation 3-3

$$CO_2 \leftrightarrow CO - \frac{1}{2}O_2$$

Equation 3-4

$$CO_2 + H_2 \leftrightarrow CO + H_2O$$

Due to the presence of residual exhaust gas in the cylinder at the end of the exhaust stroke mixing with the fresh fuel/air mixture being inducted into the cylinder, Equation 3-2 will change form with some of the gas species in the exhaust gas forming part of the reactants of the equation. Equation 3-2 then becomes:

Equation 3-5

$$C_xH_y + aO_2 + bN_2 + cH_2O + dH_2 + eCO_2 + fCO \rightarrow gCO_2 + hH_2O + iN_2 + jCO + kO_2 + lH_2$$

The molar concentrations in Equation 3-5 are dependant on the type of fuel and the operating conditions of the engine.

3.1.2 Mass fraction burned- functional descriptor

Mass fraction burned x_b is determined from the analysis of the measured pressure obtained from the experimental data. It has been shown that the mass fraction burned has a characteristic S-shape curve with respect to crank angle degree. Mass fraction burned is defined by Equation 3-6.

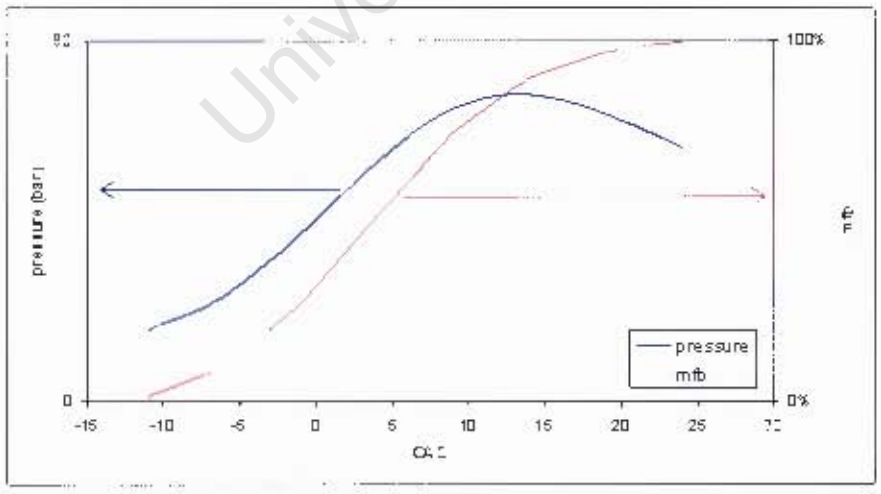

Figure 3-1: Analysis of pressure data to determine mass fraction burned

Equation 3-6

$$x_b = \frac{m_b}{m_{total}}$$

In this work a Wiebe function shown in Equation 3-7, has been used to describe the generic mass fraction burned (Heywood, 1988):

Equation 3-7

$$x_b = 1 - \exp\left[-a\left(\frac{\theta - \theta_o}{\Delta\theta_b}\right)^{m+1}\right]$$

Where a and m are variables obtained by fitting the calculated pressure profile to the experimental data.

3.1.3 Engine breathing

The gas exchange process was modelled as a quasi-steady process, where all flow was assumed to be incompressible, and the gas was assumed to obey the ideal gas law.

Exhaust manifold pressure was assumed to be constant throughout the exhaust process.

The slight pressure drop which occurs in the inlet manifold pressure was dependant on the resistance elements in the system, the cross-sectional area in which the gas travels, and the inlet density. The pressure drop in the inlet manifold is governed by the geometry of the manifold and the inlet conditions and is shown in Equation 3-8. The inlet manifold temperature was assumed to be constant during the induction process. The formulation of Equation 3-8 is shown in the Appendix A-2.

Equation 3-8

$$\Delta P_{man} = \left(K_{in} + \frac{4FL}{D}\right) \cdot \tfrac{1}{2} \rho_{man} v_{man}^2$$

3.2 Boundary layer theory and modelling

3.2.1 Thermal boundary layer

The thermal boundary layer is defined as the layer of fluid adjacent to a heated or cooled surface where significant temperature gradients are present in the fluid between the free fluid temperature and wall surface temperature. (Holman, 2002)

Modelling of the thermal boundary layer in a motored engine has been described by Lawton (1987) in a study to show how the compression and expansion of gas in a cylinder of an internal combustion engine affects the instantaneous heat transfer rates. Lawton showed that the heat flux flowed from the gas to the cylinder walls and this condition could persist even

when the bulk gas temperature was lower than the wall temperature. Similarly the gas lost heat to the wall even when the bulk gas temperature was higher than that of the cylinder walls at the time. Lawton used the conservation of energy in the form shown in Equation 3-9 to determine the effects of compression and expansion on heat transfer.

Equation 3-9

$$\frac{\partial T}{\partial t} = \alpha \frac{\partial^2 T}{\partial x^2} - \frac{\gamma - 1}{V} \cdot \frac{\partial V}{\partial t} T = 0$$

Lawton subsequently deduced that the temperature in parts of the boundary layer could be higher than the bulk gas temperature due to the initial temperature profile before compression, and visa-versa during expansion, as illustrated in Figure 3-2. Lawton's work showed that during expansion a distinct cool region is formed just adjacent to the wall even when the bulk gas temperature is much higher than the wall temperature, leading to an S-shaped temperature distribution. A numerical solution of Equation 3-9 by Lawton is provided in the Appendix A-3.

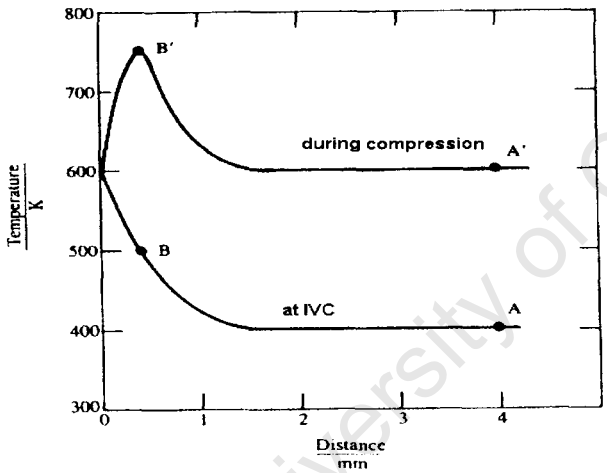

Figure 3-2: Figure showing the effect of compression on the temperature profile in the boundary layer of a SI engine during compression

Thermal boundary layers in firing spark ignition engines have been measured by Lyford-Pike and Heywood (1984). They found the thickness of the thermal boundary layer to be around 2mm – 3mm at times and could contain about 20 – 30% of the charge mass during combustion. They stated that the thermal boundary layer thickness was dependant on the thermal diffusivity of the gas and the time needed for the boundary layer to develop. They developed an expression which related the boundary layer thickness to the Reynolds number, which agreed well with the data they had gathered from their measured results. (See Equation 3-10, Equation 3-11 and Equation 3-12)

Equation 3-10

$$\delta_T = 0.6\,\mathrm{Re}^{0.2}\sqrt{\alpha t}$$

Where:

δ_T = thermal boundary layer thickness

α = thermal diffusivity

t = time measured from TDC

The Reynolds number was calculated as:

Equation 3-11

$$\mathrm{Re} = \frac{\rho v x_0}{\mu}$$

Where ρ, v, μ are the gas density, velocity and viscosity respectively. All gas properties were assumed to be constant through the cylinder volume. It was also assumed that the gas velocity had a linear relationship with the piston velocity with respect to the piston position, defined by Equation 3-12:

Equation 3-12

$$v = v_p\left(\frac{x_0}{x}\right)$$

Where

v = gas velocity

v_p = piston velocity

x = distance between piston head and cylinder head

x_0 = distance at which boundary layer thickness is calculated from cylinder head

The validity of the Lyford-Pike and Heywood formulation was limited to conditions when the distance x_0 was greater than two-thirds the clearance height. From Equation 3-10 it follows that the thermal boundary layer would approach zero at TDC as the mixture is burning, and should thicken during the expansion stroke because of the downward motion of the piston creating a downward axial velocity.

3.2.2 Momentum boundary layer

Jenkin et al (1996a) noted that the thermal boundary layer away from the cylinder wall is outside the influence of the velocity boundary layer, suggesting that the velocity boundary layer is smaller than the thermal boundary layer. This is not surprising since conventional boundary

theory over flat plates indicates that the thickness ratio between the velocity and the thermal boundary layer is:

$$\frac{\delta}{\delta_T} \approx \mathrm{Pr}^n$$

The limit of this ratio is approximately 1 for gases. (Aparci and Larsen, 1984)

Foster and Witze (1987) measured the velocity close to the wall of a combustion chamber in a motored engine, and concluded that the velocity profile in a high swirl engine approaches a typical turbulent 1/7th power law. Hall and Bracco (1986) also measured velocity in the cylinder of a SI engine and found that, prior to combustion, the bulk velocities in a fired cycle closely follow those from a motored cycle but deviate from this at the onset of combustion, and return to the motored cycle values during expansion. Average gas velocities in the cylinder are discussed in chapter 3.3.3.

3.3 Heat transfer modelling along the length of the thermocouple

Empirical heat transfer modelling is based on classical steady-state and unsteady-state heat transfer formulations. The values of the variables used in this section were determined from the data gathered from test results.

3.3.1 Steady state heat transfer

Conduction heat transfer

When a temperature gradient exists within a body, energy transfer by conduction occurs within the body from the region of high temperature to the region with a lower temperature, and the rate of energy transfer per unit area is proportional to the temperature gradient.

$$\frac{q}{A} \propto \frac{\partial T}{\partial x}$$

The rate of heat conduction is defined as k, the thermal conductivity in Fourier's equation for heat conduction.

Equation 3-13

$$q = -kA\frac{\partial T}{\partial x}$$

Convection heat transfer

Convection heat transfer is the diffusion of heat energy in a moving deformable medium. Convection heat transfer per unit time is expressed in terms of a heat transfer coefficient h, according to Newton's law of cooling. This is shown in Equation 3-14

Equation 3-14

$$q = hA(T_g - T_w)$$

3.3.2 Unsteady state heat transfer

When a solid body such as a thermocouple probe is subjected to a sudden change of environment, some time will elapse before a state of equilibrium is achieved. Research in this project made use of the lumped heat capacity method to calculate transient heat conduction. The lumped heat capacity method assumes that the internal heat transfer resistance of the body is small compared to the external resistance, so temperature gradients within the body can be ignored. So heat loss or gain is governed by the change in the body's internal energy.

Equation 3-15

$$q = mC_p \frac{dT}{dt}$$

3.3.3 Heat transfer through the thermocouple

It is shown in chapter 2.2 that thermocouples have a slow response to the transient environment in a cylinder of an SI engine. A model was developed to estimate the change of temperature of the thermocouple throughout the engine cycle, taking into account the effect of the heat conduction to the wall of the cylinder, and the convection from the flowing gas in the cylinder to the change in thermocouple temperature. The model assumed one dimensional conduction along the length of the thermocouple.

The numerical model used in the project for estimating the heat transfer along the thermocouple was based on classical steady state heat transfer and local lumped heat capacity theory. The thermocouple was analysed in small elements as shown in Figure 3-3 and the basic formula used to calculate heat transfer in each of the elements is shown in Equation 3-16.

Equation 3-16 caters for convection and conduction into and out of the element, and an unsteady term that caters for the transient environment within the cylinder.

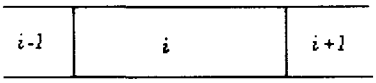

Figure 3-3: Picture of thermocouple elements

Equation 3-16

$$hA_s(T_g - T_i) - kA_c\frac{T_i - T_{i+1}}{\Delta x} - kA_c\frac{T_{i-1} - T_i}{\Delta x} - mC_p\frac{dT}{dt} = 0$$

The convection coefficient, h in Equation 3-16 was calculated using the Nusselt number empirically modelled for a situation with a cylinder and gas flowing across it. The relationship between the Nusselt number and the convection coefficient is:

Equation 3-17

$$Nu = \frac{hd}{k_f}$$

Holman (1997)

Where the Nusselt number is calculated from:

Equation 3-18

$$Nu = \left(a + b \cdot \mathrm{Re}^{c}\right)\mathrm{Pr}^{d}$$

Where a to d are variables which are inferred for different situations.

Equation 3-19

$$\mathrm{Re} = \frac{\rho_f v d}{\mu_f}$$

The Reynolds number 'Re' for each element is calculated using gas properties at the film temperature (subscript f) which are assumed to be constant for the element.

The velocity values, v used in the calculation of the Reynolds number were modelled by Hsiao (2006). Using CFD to provide ensemble averaged velocities in the CFR engine. This analysis was undertaken for the intake and compression strokes across the cross-section of interest to this particular project, in the clearance volume. High velocities were generated during the intake stroke, reaching a maximum value and steadily declining due to piston motion and falling even further during the compression stroke as shown in Figure 3-4. Hsiao showed that the average gas velocity across the cross section increases with compression ratio.

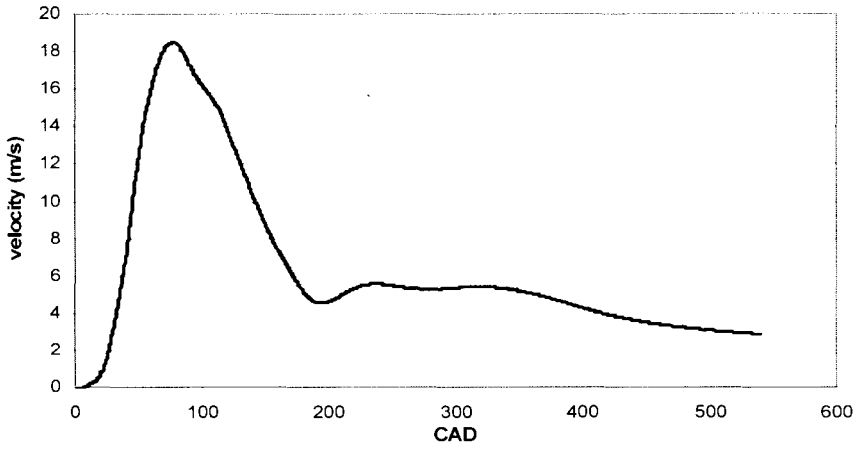

Figure 3-4: Gas velocity inside the cylinder as modelled by Hsiao (2006)

The general shape of the velocity profile and the velocity values could be confirmed by typical values available from measurements by other researchers. Heywood (1988) showed that the velocity through the inlet valve is proportional to the piston speed, and thus the in-cylinder velocities could be scaled using the mean piston speed. Figure 3-5 below shows ensemble-average mean velocities normalised using the average piston speeds, measured in the path of the intake flow that were presented by Heywood (1988). All the curves follow approximately the same shape and magnitude, supporting the decision to use this method to estimate average gas velocities at other engine speeds.

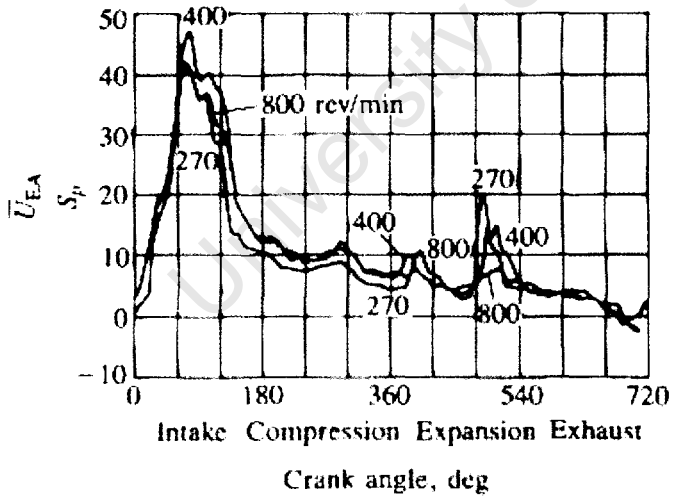

Figure 3-5: Mean velocity profiles normalised by mean piston speed, for different engine speeds

4. Experimental Procedure

Experiments for this project were conducted using a single cylinder CFR (Co-Operative Fuel Research) engine. This section describes the structure and manufacture of the thermocouples used for experiments, and the setup of the engine while doing the experiments. The different sets of data recorded and method of analysis are also described.

4.1 Thermocouple and engine setup

The numerical model developed was used to select an appropriate diameter and length of thermocouple. An unsheathed K-type thermocouple was used in this project.

4.1.1 Manufacture of Thermocouple

Initially a sheathed thermocouple was purchased. The tip of the stainless steel sheath was cut away to expose the thermocouple wires. The exposed wires were then cut to the desired length out of the sheath and welded together. After welding, the blob formed by the fusion of the thermocouple wires had to be ground away until it was approximately the same thickness as the thermocouple wire. This was done to reduce the mass of the hot junction and allow for modelling simplicity.

Figure 4-1: Figure showing how the thermocouple junction was formed

One of the finished thermocouples is shown in Figure 4-2.

Figure 4-2: Picture showing a magnified image of the 2mm long, unsheathed thermocouple

The exposed thermocouple was fitted into a holder that was specially designed to fit into the spark plug hole of the CFR engine, while housing the thermocouple. The thermocouple was silver soldered to the holder to ensure good thermal contact between the cylinder wall and the thermocouple. The thermocouple was soldered in such a way that the edge of the cut-away sheath was flush with the holder, in the hole marked 'A' in Figure 4-3, thereby exposing the full length of the thermocouple wires to the flowing in-cylinder gases.

Figure 4-3: Image of thermocouple holder

The wall temperature was measured using a second thermocouple embedded in the thermocouple holder in close proximity to the thermocouple which was attempting to measure the gas temperature. The second thermocouple was fitted in the hole marked 'B' in Figure 4-3. This was done in a bid to ensure that the wall temperature values used in the model were as close to reality as possible. The method used in embedding the thermocouple, while ensuring that the thermocouple junction was as close to the surface as possible, was the same technique used by Enomoto et al (1997), shown in Figure 2-4. Wall temperature fluctuations

were discounted for modelling work because they were considered to be negligible, so wall temperature was assumed to be constant throughout the cycle.

An image of the final thermocouple assembly is shown in Figure 4-4 below.

Figure 4-4: Image of thermocouple in holder, also showing position of the thermocouple embedded in holder

4.1.2 Setup on CFR engine

The thermocouple holder was located in one of the spark plug holes on the side of the engine in the clearance volume. The spark plug was moved to the top of the engine and fitted in the aperture where the knock sensor would normally be fitted. The engine was also equipped with a crank-angle encoder. A laminar flow meter was fitted in front of the intake manifold to measure mass of the air inducted into the engine cylinder. A National Instruments NI DAQ card was used to capture all the signals from the different transducers simultaneously and assigning them to the appropriate crank-angle degree. All the signals were read via a computer interface in National Instruments LabVIEW™, and then converted to spreadsheet format for analysis.

4.2 Experiments on the CFR engine

Experiments for this project were conducted on the CFR engine while motoring and firing. Basic dimensions of the CFR engine are shown in Table 4-1. Motored tests were conducted for the purposes of calibrating the model, and the data acquisition for processing the data from the fired engine cycles.

Table 4-1: Basic dimensions of single cylinder CFR engine

Item	Value
Bore (mm)	*82.55*
Stroke (mm)	*141.3*
Compression ratio	*variable*
Engine speed	*variable*
IVO (CAD)	*-350*
IVC (CAD)	*-146*
EVO (CAD)	*140*
EVC (CAD)	*-345*

Measurements were done on the CFR to acquire all data needed to enable full analysis of the measured temperature in the thermocouple. Besides the temperature of the thermocouple in the gas stream being recorded, the cylinder pressure, wall temperature and equivalence ratio in the case of fired engine cycles were recorded. The temperature, the absolute pressure, and the differential pressure at the laminar flow meter were also recorded.

4.2.1 Motored tests

Motored tests were run for the different protrusion lengths of thermocouples at different test conditions, with varying engine speed, compression ratio. Mass intake into the engine was calculated using the differential pressure measured across the laminar flow meter at the inlet manifold of the engine. The density of the air passing through the laminar flow meter was calculated from the measured gas temperature and the measured absolute pressure.

Table 4-2 shows the range of conditions at which the tests were run.

Table 4-2: Engine conditions when the engine is being motored

Engine speed	Compression Ratio	Induction pressure
rpm	-	Bar
300 – 900	*5.5 – 7.0*	*~1.0 (atmospheric pressure)*

A linear relationship exists between the differential pressure across the laminar flow meter and the volume flow rate through it. Due to the nature of the flow dynamics in the inlet manifold of the engine the drop in pressure across the laminar flow meter lagged the inlet stroke. This phenomenon is shown in Figure 4-5. In light of the transient characteristics of the pressure drop, it was reduced to its mean value over the complete engine cycle and the volume flow rate and mass flow rate were calculated as follows.

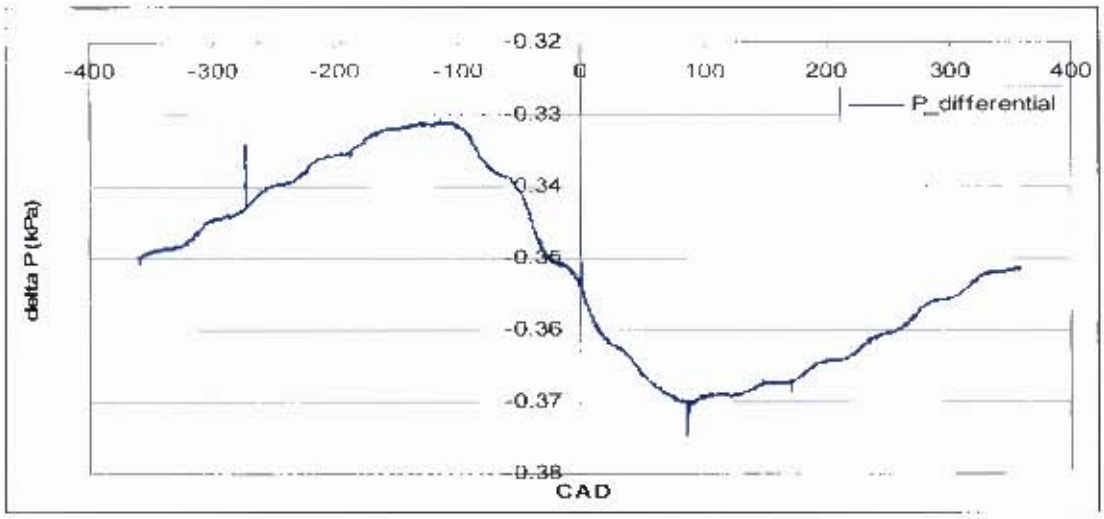

Figure 4-5: Differential pressure through the inlet manifold

$\dot{V} = a\Delta P - b$ m^3/s

$\dot{m} = \dot{V}\rho_{in}$ kg/s

where:

$\rho_{in} = \frac{P_{abs}}{RT}$ kg/m^3

$m = \dot{m} \cdot \Delta t$ kg

Δt is the time period which the inlet valve is open.

The equations above show the simple calculation of the mass inducted into the cylinder of the engine.

The measured pressure values from the motored engine cycle were modelled and verified using the technique described in chapter 3.1. Comparison of a typical measured pressure trace to a modelled trace from a motored engine cycle is shown in Figure 4-6.

Verification of the set compression ratio and locating the actual TDC point in the acquired data was done by calculating the instantaneous polytropic coefficient. For fresh air, as is the case with the motored engine the polytropic coefficient for isentropic compression was expected to be approximately 1.4. The polytropic coefficient k, was calculated using Equation 4-1.

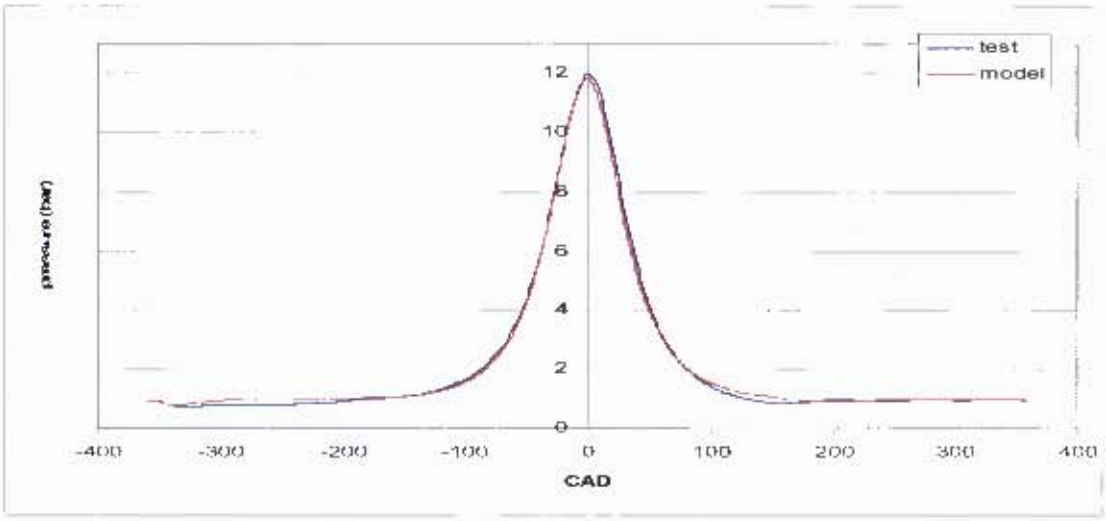

Figure 4-6: Comparison of measured and modelled motored pressure at 600rpm and compression ratio 6.0

Equation 4-1

$$k = \frac{\log\left(P_1 / P_2\right)}{\log\left(V_2 / V_1\right)}$$

A result of the ensuing calculation is shown is Figure 4-7. The figure shows the polytropic coefficient approaching the ideal value of 1.4 at approximately -50 CAD and again at +50 CAD. In the vicinity of TDC the polytropic coefficient has an asymptotic behaviour with the value going towards $\pm\infty$, as momentary constant temperature, constant pressure and constant volume conditions are encountered successively approaching TDC.

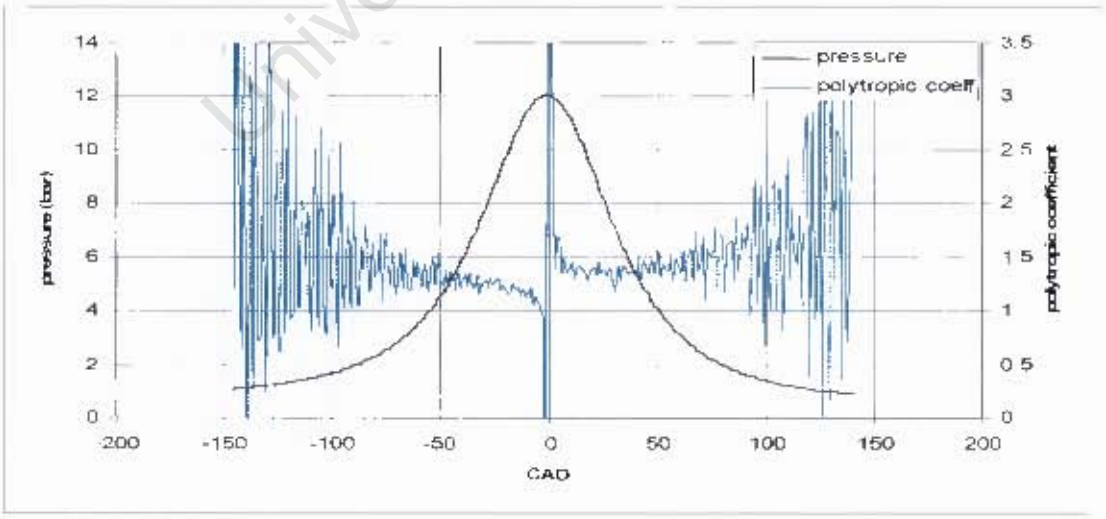

Figure 4-7: Trace showing a calculated value of the polytropic coefficient

Temperature values recorded from the measurement of the gas temperature initially experienced some signal noise, but this was remedied by passing the raw signal through a low-pass filter, and applying a smoothing function to the acquired data. Two types of averaging functions were used for smoothing the recorded data; the rectangular average, which replaces each point in the signal with the average of the adjacent points, and the triangular average, which is a weighted smoothing function. Figure 4-8 shows a typical temperature trace of the thermocouple in a motored engine, with the smoothing function applied over it.

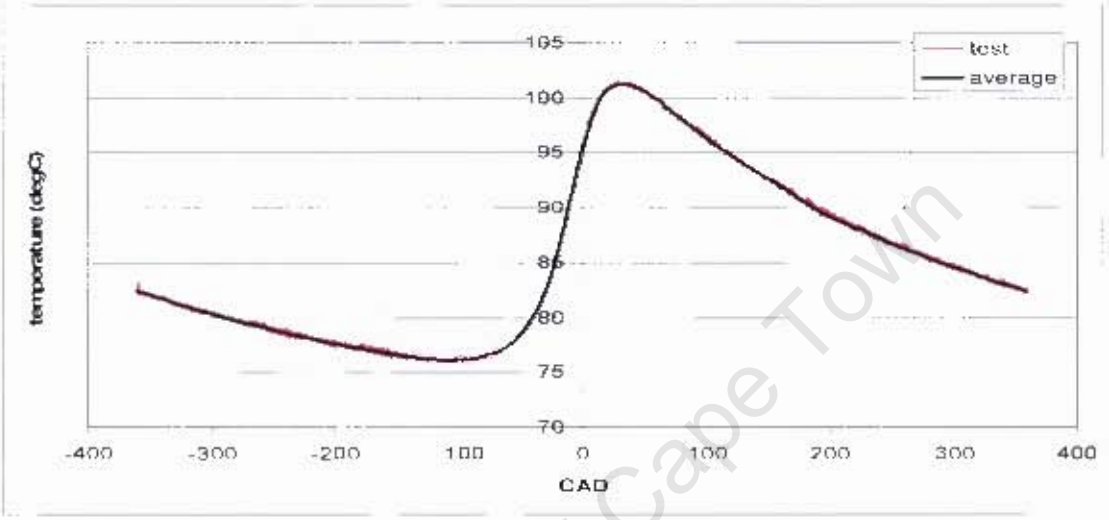

Figure 4-8: Measured temperature trace with and averaging function on it

4.2.2 Fired tests

Tests were conducted on the CFR engine using 95 Octane unleaded petrol from the market. Fired tests were run on the engine for varying engine speeds, compression ratios and air/fuel ratios. There were some limiting factors as to which test could be run and these associated with the lean burn limits, and turbulence at low engine speeds.

Table 4-3: Engine setup conditions when firing the engine

Engine speed	Compression Ratio	Induction pressure	Fuel type	λ	Spark timing
rpm	-	bar	-	-	CAD
300 – 900	*5.5 – 7.0*	*~1.0*	*95 unleaded*	*1.0 – 1.2*	*13.4 BTDC*

Most of the tests were run with fuel/air mixtures leaner than stoichiometric in a bid to try and reduce the average temperatures of the gas cylinder. This was done in the hope of reducing the overall heat transfer to the thermocouple and thus achieving a minimum thermocouple temperature before the spark.

An ideal gas law was not assumed when modelling the fired engine. Because of the gas composition, the polytropic coefficient and the gas constant could not be assumed to be

constant. Thus the model described in chapter 3.1 was used to simulate combustion, using measured values of volumetric efficiency and wall temperature the modelled pressure would be compared to the measured pressure trace. This is shown in Figure 4-9. The temperature values were also calculated using the same model.

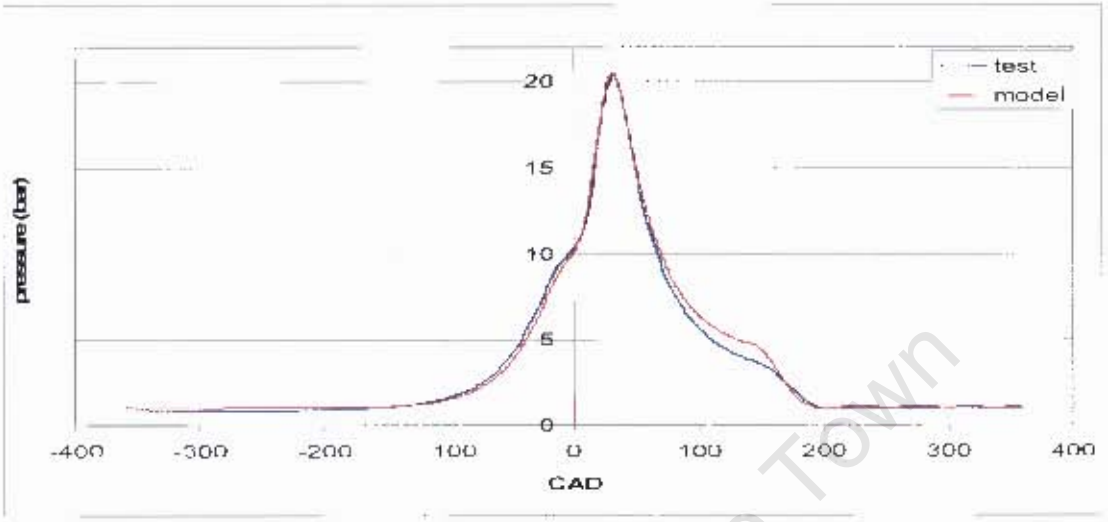

Figure 4-9: Simulation of test pressure done at 600rpm, compression ratio 5.5 and lamda value 1.20

4.3 Modelling engine cycle and heat transfer to thermocouple

Modelling the engine cycle for the analysis of results was based on the measured cylinder pressure and the measured mass inducted into the engine with an estimate of the residual gas mass. These were used to estimate an average gas temperature for the compression and the expansion strokes using the ideal gas law. An example of this method applied to a motored cycle is shown in Figure 4-10.

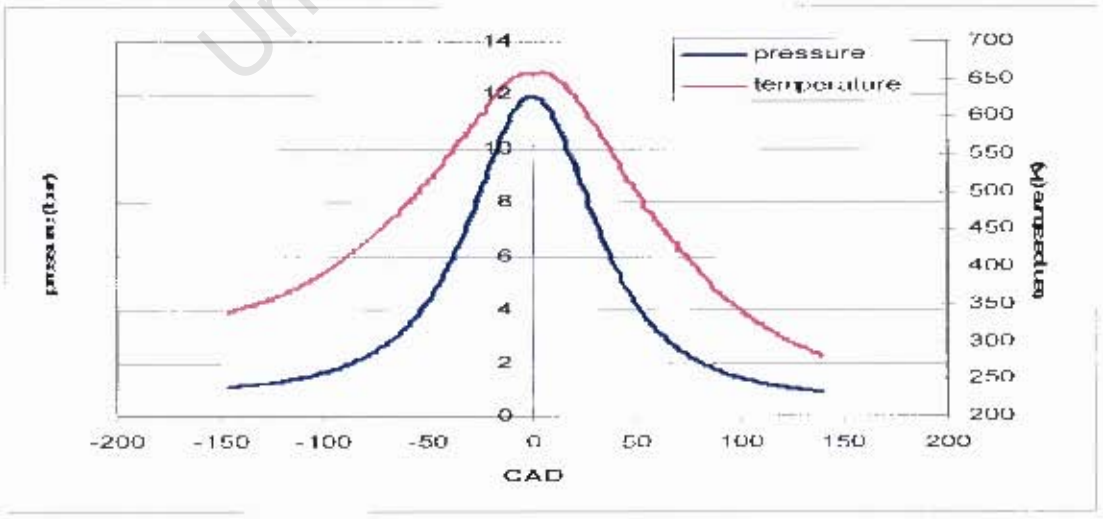

Figure 4-10: Trace showing measured cylinder pressure and temperature calculated using the ideal gas law for a motored engine

As can be seen in Figure 4-10 the values of pressure and temperature at EVO are about 50°C lower than the starting values at IVC. This is due to heat loss occurring during compression and expansion cycles.

The conditions at EVO were used as the starting conditions for the breathing cycle. The quasi-steady model described in chapter 3.1.3 was used to model the breathing cycle. The piezo-electric pressure transducer used for this work tended to drift when changes in pressure were small. This was remedied by conditioning the transducer in an oven for 24 hours to remove any moisture that might have been altering the charge signal. Several iterations of the model were run until the conditions at IVO produced by the model matched those from the measured pressure signal. From this, a value of residual gas mass was estimated and was used for calculations.

Once a bulk cylinder gas temperature was calculated a temperature profile for the thermal boundary layer could be modelled. Heat transfer along the length of the thermocouple was iterated until a state of equilibrium was attained by the model over the full engine cycle. The thermophysical properties of the thermocouple material used were found in a publication by Sundqvist (1992), who did research on the thermal conductivity and diffusivity of the Chromel and Alumel in the temperature range of interest in this project. The result produced by the model was compared to the measured temperature profile to ascertain the accuracy of the heat transfer model.

5. Results

This section presents the results obtained during the testing phase of this project. Results are presented from the long thermocouple in the bulk gas of the cylinder, and both the 2mm and the 4mm thermocouples in the thermal boundary layer. These selected results show the trends of the thermocouple and the effect of changing parameters such as engine speed, compression ratio and thermocouple length. The measured results were compared to the estimated bulk gas temperatures to assess the accuracy and validity of the measuring technique.

5.1 Engine test results in the bulk gas

Results measured from the bulk gas of the cylinder are shown in the following graphs. Temperature measurements in the bulk gas stream were done with thicker thermocouple wires, and with varying protruding lengths.

The results of the longer thermocouple exceeding 20mm were not affected significantly by the length of the thermocouple, a difference of approximately 4 degrees is shown from a protrusion length of 20mm to 30mm, and the swing of the thermocouple temperature is almost identical at approximately 12 degrees. This is probably because the convection in the bulk of the cylinder gas is uniform, and the effect of conduction from the wall is negligible. This shows in effect that as the thermocouple gets longer, the effect of conduction from the wall gets less, and the gas convection becomes dominant.

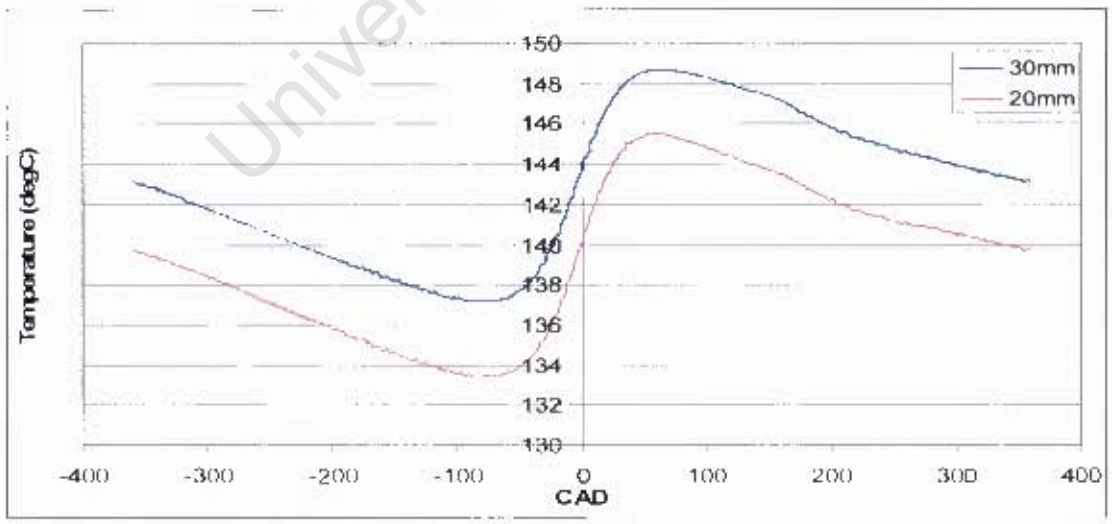

Figure 5-1: Graph comparing temperature measurements using the longer thermocouple at different lengths, at 300rpm and 7.0 compression ratio.

Measurements with the long thermocouple were also compared to the bulk gas temperatures; this is shown in Figure 5-2. It can be seen from the figure that the range of the thermocouple

temperature swing is relatively small compared to the gas temperature variation. Figure 5-3 zooms in on the thermocouple temperature highlighting the points where it intercepts the bulk gas temperature and the thermal equilibrium points. It can be seen that the thermocouple tracks the gas temperature quite reasonably. The minimum and maximum temperatures of the thermocouple are almost matched to the bulk gas temperatures at that particular crank angle degree. The discrepancies could be accounted for by the physical properties of the thermocouple which cause a slight time lag, and it may also be due to a local boundary layer forming around the thermocouple wires.

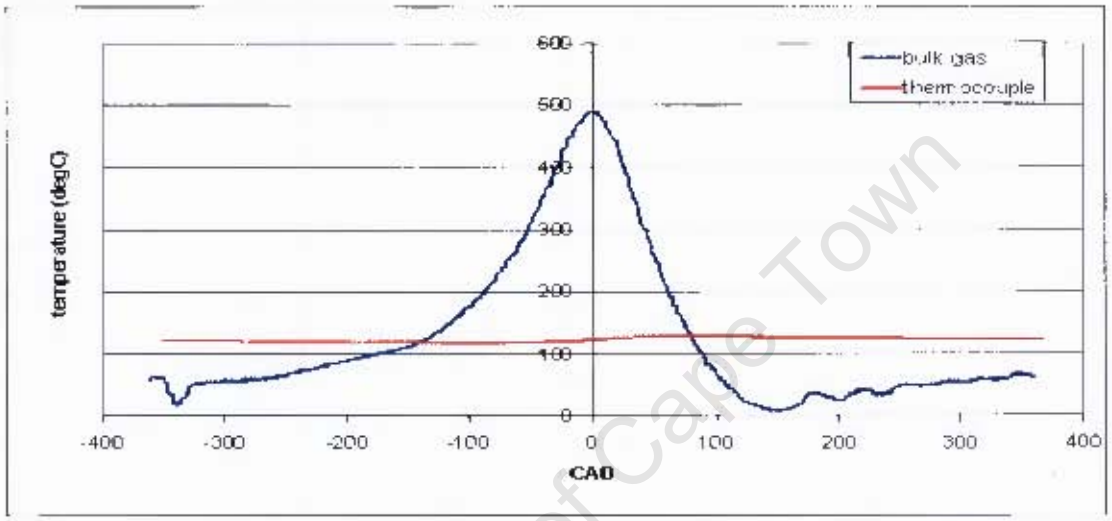

Figure 5-2: Thermocouple temperature compared to bulk gas temperature

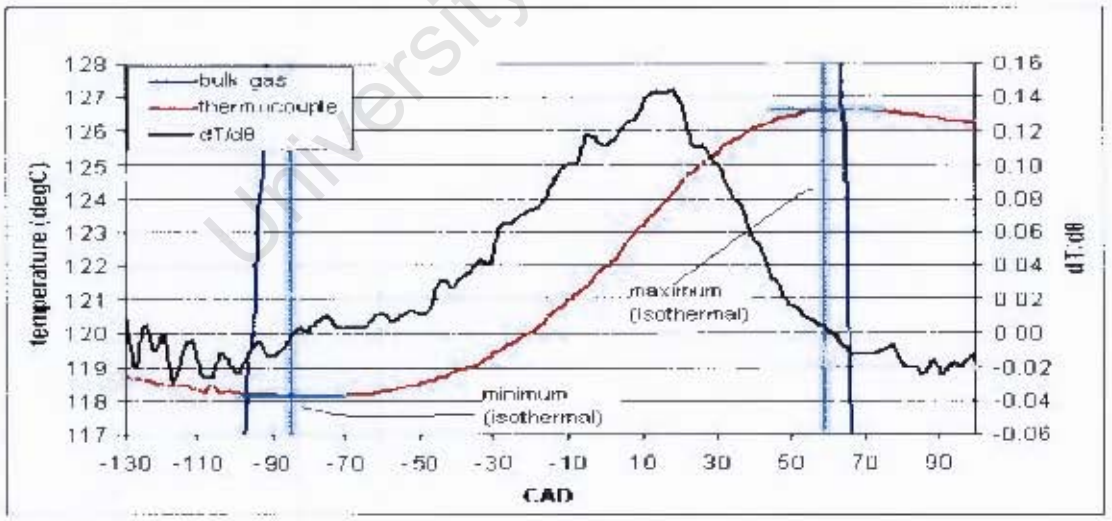

Figure 5-3: Graph showing the measured thermocouple temperature against the estimated bulk gas temperature at 300rpm and compression ratio 6.0 with the 30mm thermocouple

Figure 5-4 shows a temperature trace from a fired engine using the long thermocouple. The trace shows that the minimum temperature occurs after the TDC, and that the thermocouple has an average value of around 700°C, which is the average gas temperature throughout the

cycle. It was noted that the thermocouple was not responding fast enough to the changes in gas temperature to have the minimum gas temperature before the spark occurred. Changes in thermocouple diameter to enable faster response which would move the minimum temperature closer to the spark point would have resulted in a greater temperature swing and the thermocouple possibly exceeding its melting temperature.

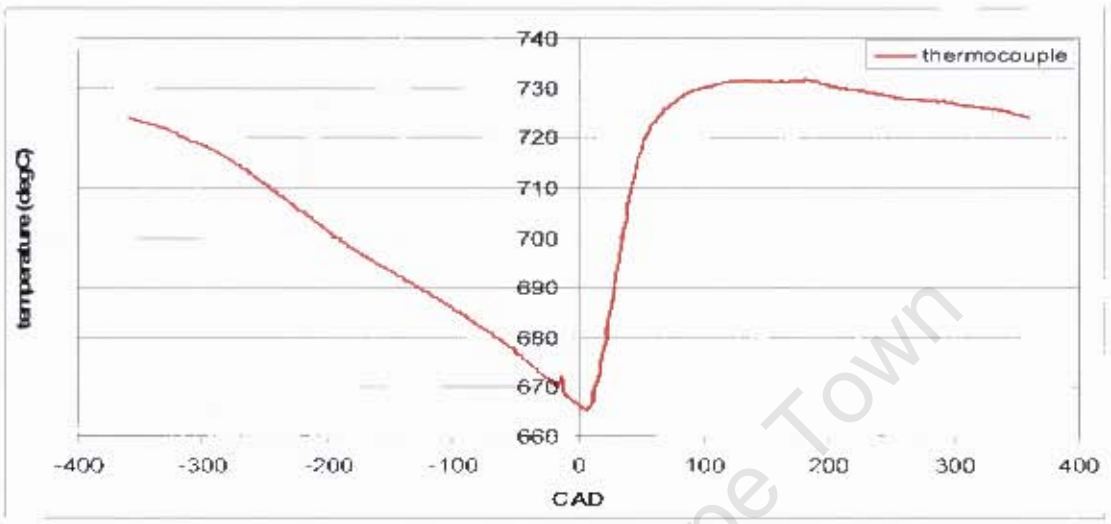

Figure 5-4: Temperature measured by a 15mm thermocouple in a fired engine at 600rpm and 5.25 compression ratio.

5.2 Engine test results in the thermal boundary layer

5.2.1 Measured temperature traces from a motored engine

Selected results obtained from the thermocouples protruding 2mm and 4mm into gas stream are presented below. Although measured results were available for a wide range of compression ratios and engine speed, the results for the 2mm thermocouple presented in Figure 5-5 show the effect of changing compression ratio at a constant speed, and the crank angle degrees at which the minimum and maximum temperatures occur. The results for the 4mm thermocouple shown in Figure 5-6 show the effect of changing engine speed. It must be noted however that all cycles were run and recorded at different wall temperatures, this has the effect of moving the thermocouple temperature graph vertically for the various data presented.

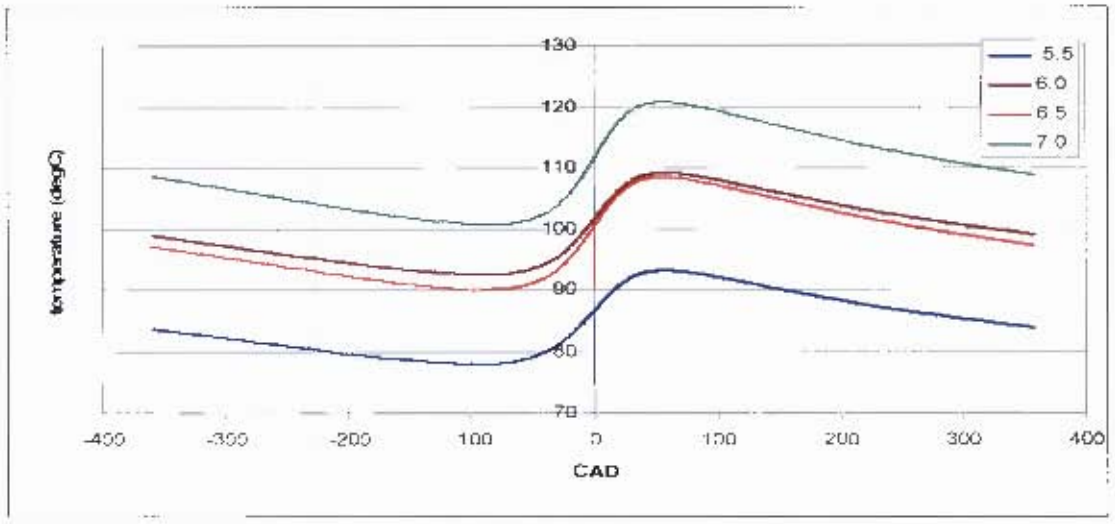

Figure 5-5: Graph showing the progression of thermocouple temperature during a motored cycle. All graphs show measurement using the 2mm thermocouple at 600rpm engine speed and different compression ratios

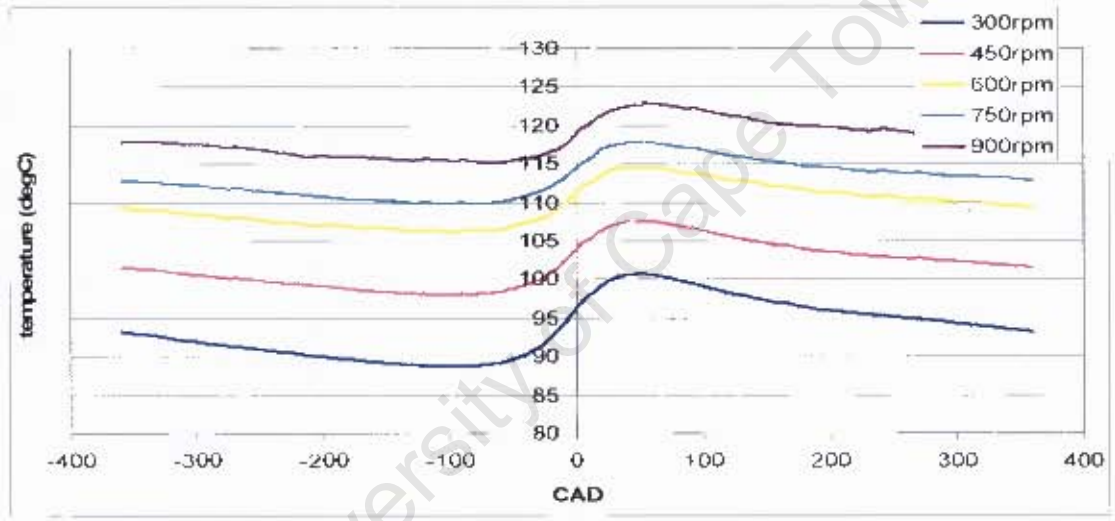

Figure 5-6: Graph showing the progression of thermocouple temperature during a motored cycle. All graphs show measurement using the 4mm thermocouple at compression ratio 6.0 and different engine speeds

It was found that while there was a discernible swing in the thermocouple temperature, in most cases it did not track the gas temperature well. It was found that for a given engine test condition the 2mm thermocouple exhibited a greater range than the 4mm thermocouple. An example is shown in Figure 5-7. this was not expected prior to testing, although this could have been due to differences in thermocouple wire thicknesses, other reasons for this are discussed in a later section.

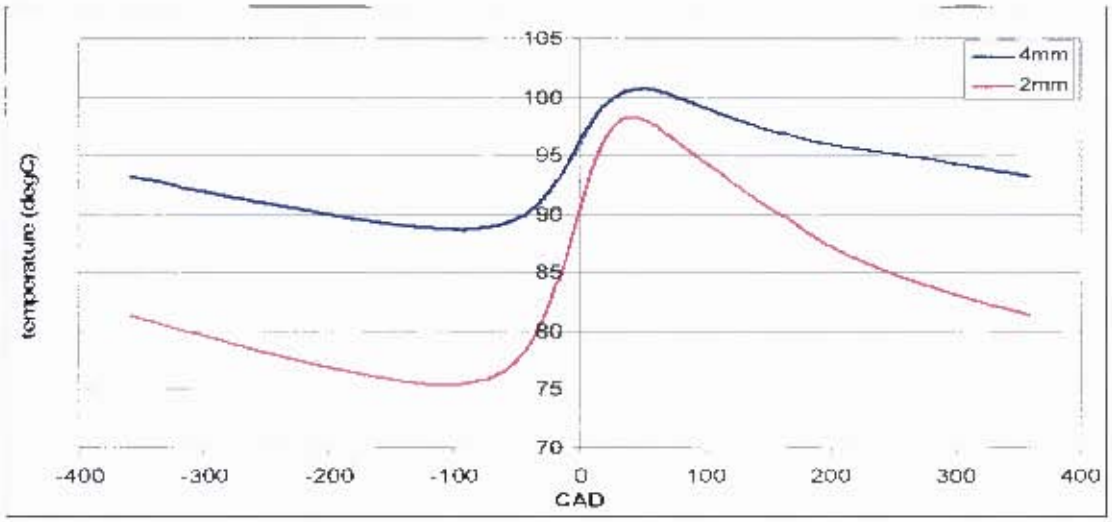

Figure 5-7: Comparison of the thermocouple temperature traces at 2mm and 4mm at the same test setting.

The temperature fluctuation measured by these thermocouples was also negligible when compared to the bulk gas. The two thermocouples are shown at the same setting in Figure 5-8 and Figure 5-9 with the annotations showing the CAD where the minimums and maximums occur. As was expected the heat transfer within the thermocouple to the cylinder wall biased the thermocouple temperature to a lower value than the bulk gas temperature.

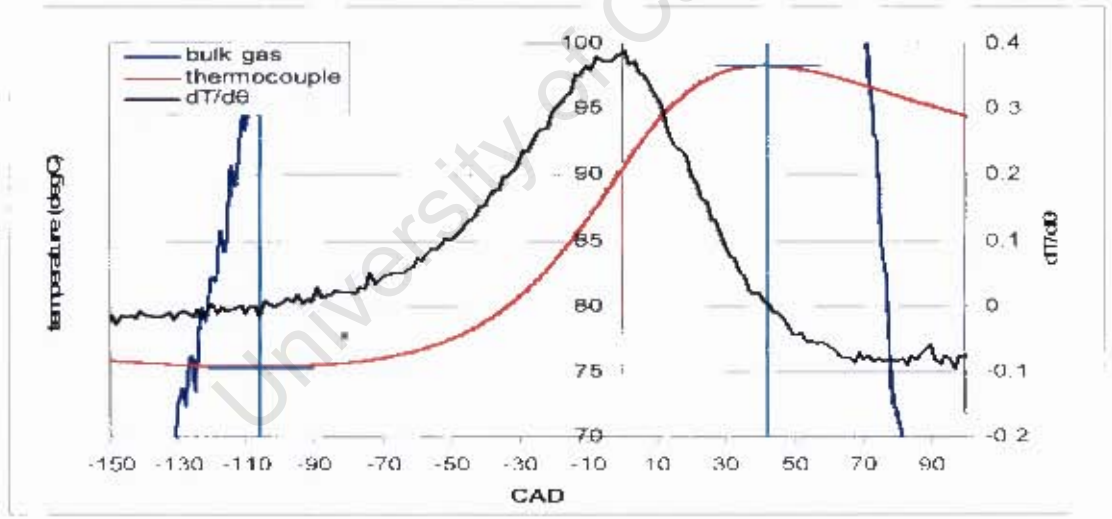

Figure 5-8: Graph showing the measured thermocouple temperature against the estimated bulk gas temperature at 300rpm and compression ratio 6.0 with the 2mm thermocouple

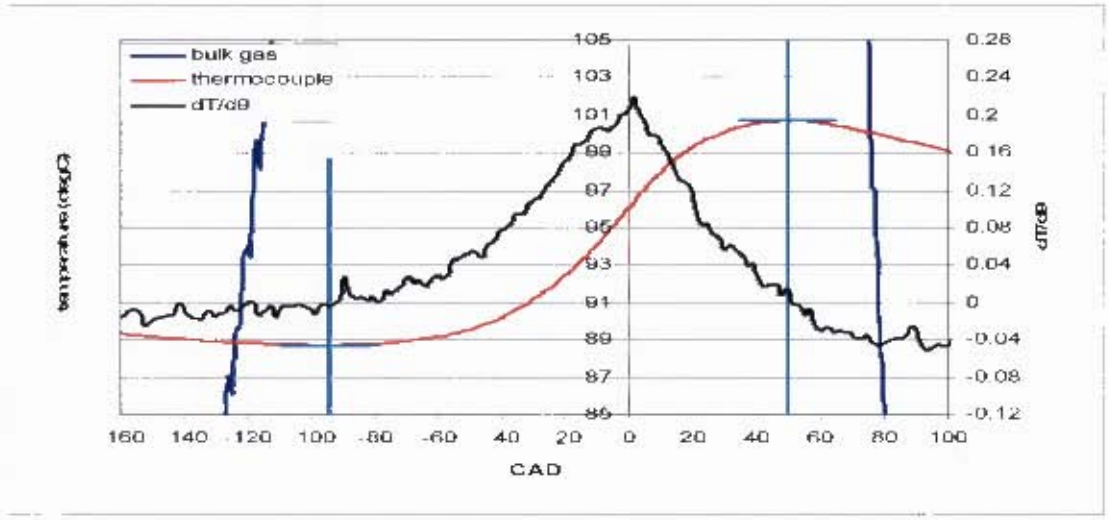

Figure 5-9: Graph showing the measured thermocouple temperature against the estimated bulk gas temperature at 300rpm and compression ratio 6.0 with the 4mm thermocouple

5.2.2 Measured temperature traces in a fired engine

A typical result from a fired engine test is shown in Figure 5-10. In order to obtain meaningful analysis it was important that the minimum temperature of the thermocouple would occur before the spark. This would enable an average gas temperature to be calculated before combustion was initiated.

Measurements were successful in as much that the minimum point occurred in the desired region. The minimum temperature in the thermocouple occurs before the spark event for the 2mm thermocouple at engine speeds of 600rpm and lower, and with compression ratios 6.0 and 5.5, and typically lambda values of 1.10 to 1.20. At 450rpm and compression ratio 5.5 results in the desired region were also achieved at stoichiometric air/fuel ratio.

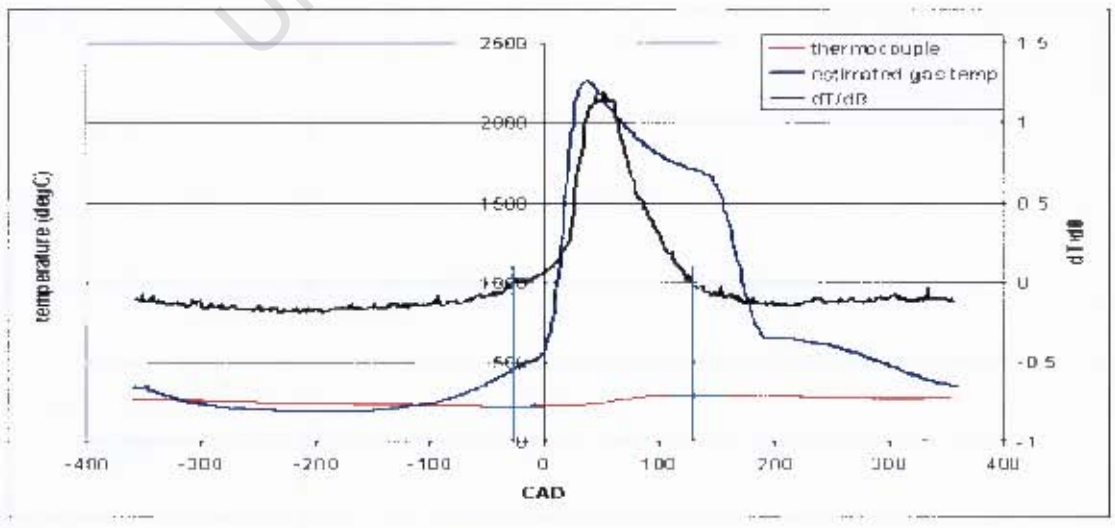

Figure 5-10: Comparison of thermocouple temperature to the modelled gas temperature

Figure 5-10 shows that the thermocouple temperature did not manage to track the bulk gas temperature sufficiently, showing small changes in thermocouple temperature when compared to changes in the simulated bulk gas temperature.

For the firing tests none of the results from the 4mm thermocouple exhibited the minimum thermocouple temperature occurring before the spark event, so those results are not presented.

6. Analysis of Results

After the results were collected, analysis was done, and the validity and usefulness of the results and methods used in assessing the results were considered. In this section the validity of the numerical model is assessed and the factors that affected the thermocouple measurements have also been considered.

Initial tests were carried out with the long thermocouple to verify the validity of the project hypothesis and the validity of the numerical heat transfer model. Figure 6-1 shows the comparison of the temperature predicted using this measurement to the calculated bulk gas temperature. From the data shown in Figure 5-3, the thermal inertia of the thermocouple caused the gas thermal profile which was inferred from the thermocouple data to exhibit an offset of about -40°C.

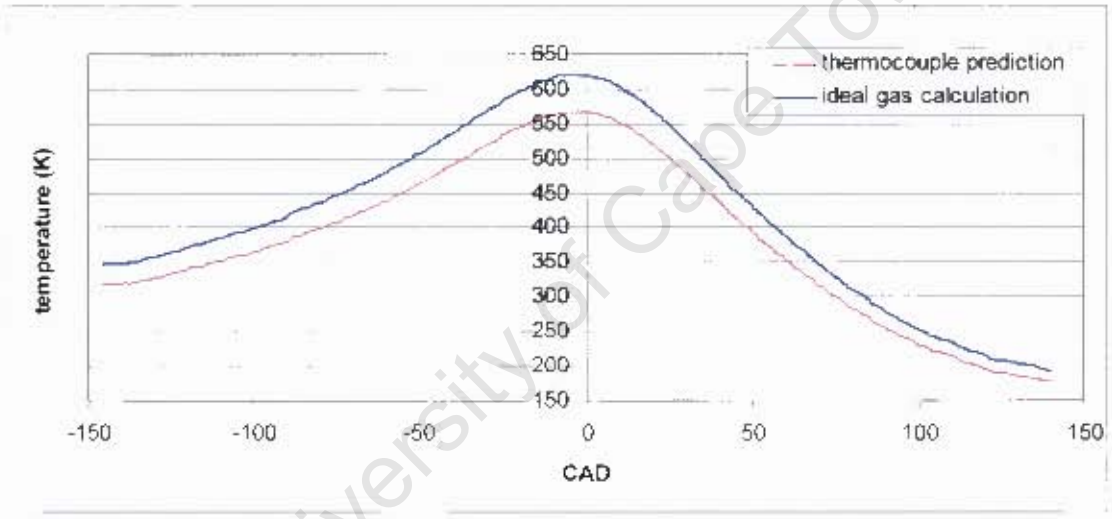

Figure 6-1: Prediction of gas temperature from the 30mm thermocouple at 300rpm and compression ratio 6.0, inferred directly from the thermocouple measurement

The thermocouple temperature prediction derived from the heat transfer model is compared to an actual measurement in Figure 6-2. The figure shows that the model prediction exhibits a nominal offset of 3°C, which is about 2% on the current thermocouple reading. On initial assessment this was thought to be satisfactory and the model was then used to design the smaller thermocouples used in the later part of the project. However it was subsequently found that the heat transfer model was grossly insufficient in predicting temperatures for the shorter thermocouples as it did not incorporate the thermal boundary layer in its calculations. A boundary layer model had to be included to calculate the temperature profile adjacent to the wall, where the thermocouples would be situated.

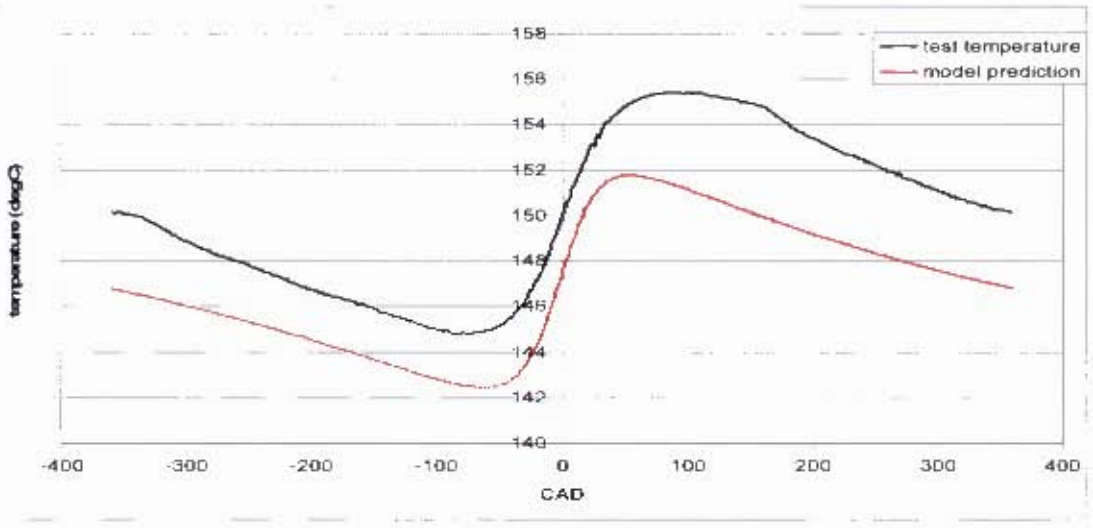

Figure 6-2: Comparison of modelled thermocouple temperature to actual measurement for a 30mm thermocouple at 400rpm

6.1 Discussion of the validity of the revised numerical model

A number of the tests conducted were used to calibrate the heat transfer model, which included the boundary layer model. This was done by modelling measured test conditions for the 2mm thermocouple only, since the results attained from the 4mm thermocouple from the fired engine were not useful for this project. The coefficients of the convection coefficient were adjusted to match the predicted thermocouple temperature profile with the measured result. Coefficients of the Nusselt number calculation in Equation 3-18 were fitted for this scenario. An example of the ensuing calculation following the model calibration is shown in Figure 6-3.

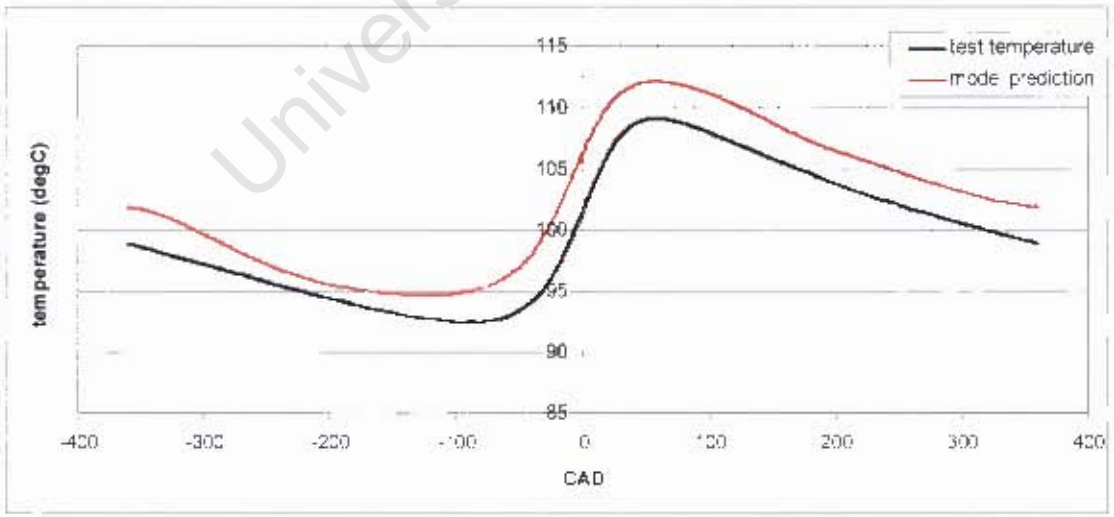

Figure 6-3: Comparison of measured temperature with the modelled thermocouple temperature at 600rpm and compression ration 6.0 using the 2mm thermocouple.

To check the validity of the numerical model that was developed, the shape of the convection heat transfer coefficient was confirmed with comparisons with global convection coefficient.

Figure 6-4 shows a global convection coefficient as predicted using the Woschni heat transfer model and the local convection coefficient for the 2mm thermocouple. While the general shape of the two graphs is similar there are obvious differences in the magnitude of the coefficients.

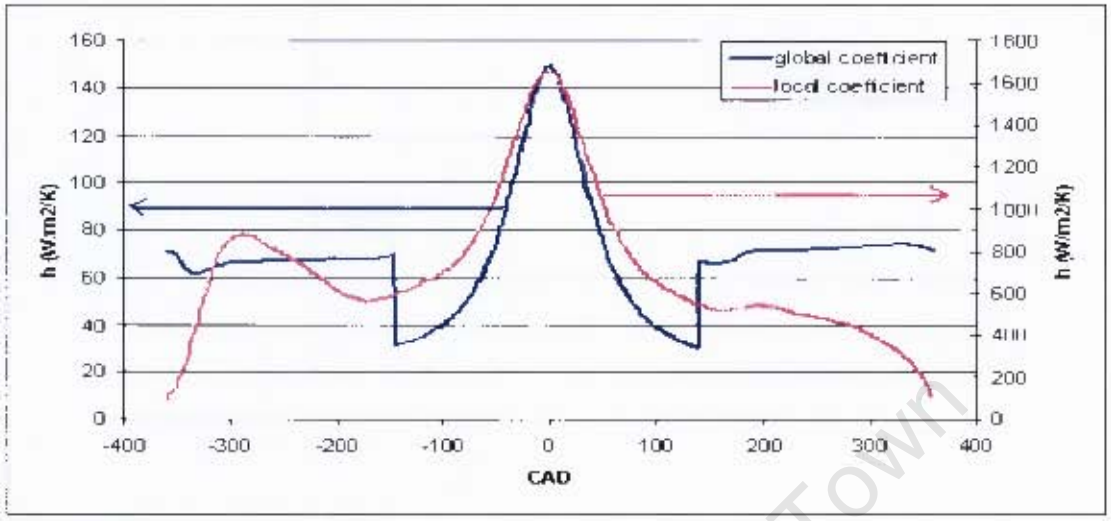

Figure 6-4: Comparison of average local convection coefficient around thermocouple with the global coefficient for the entire cylinder proposed by Woschni

The average Nusselt Number of the localised situation of the thermocouple was also plotted against the Reynolds Number. From work done by Annand, shown in Lawton (1987) and Heywood (1988), the relationship between the two numbers is governed by Equation 6-1. Figure 6-5 shows that this form was maintained even for the localised situation.

Equation 6-1

$$Nu = a \cdot \mathrm{Re}^{b} + c$$

Where 'b' is typically 0.7

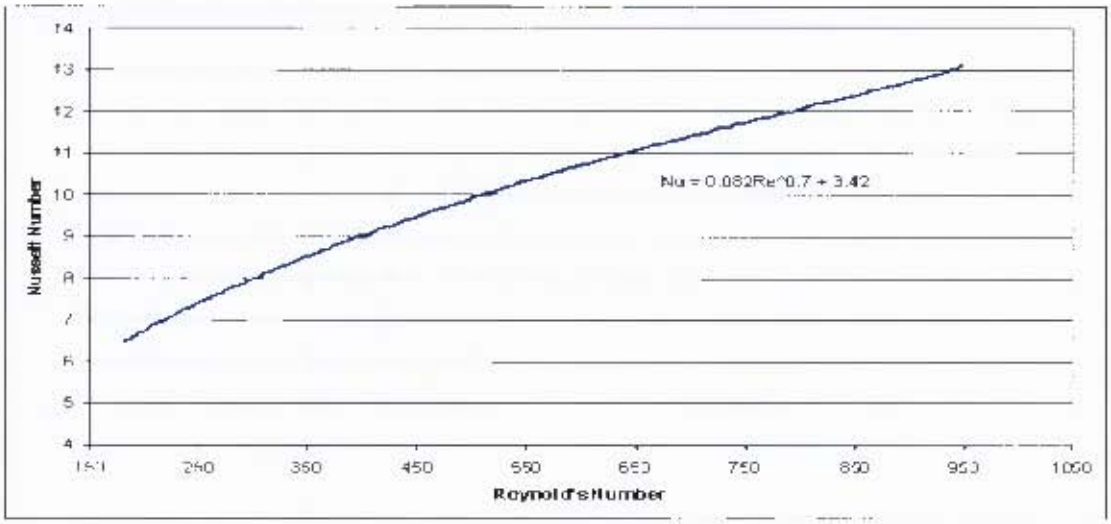

Figure 6-5: Relationship of the average Reynolds Number to the Nusselt Number around the thermocouple probe

It was found that the average convection coefficients for the situations modelled could be described by a surface shown in Figure 6-6. The surface could be closely approximated by Equation 6-2, and this was used to estimate the average convection coefficients for the other test conditions.

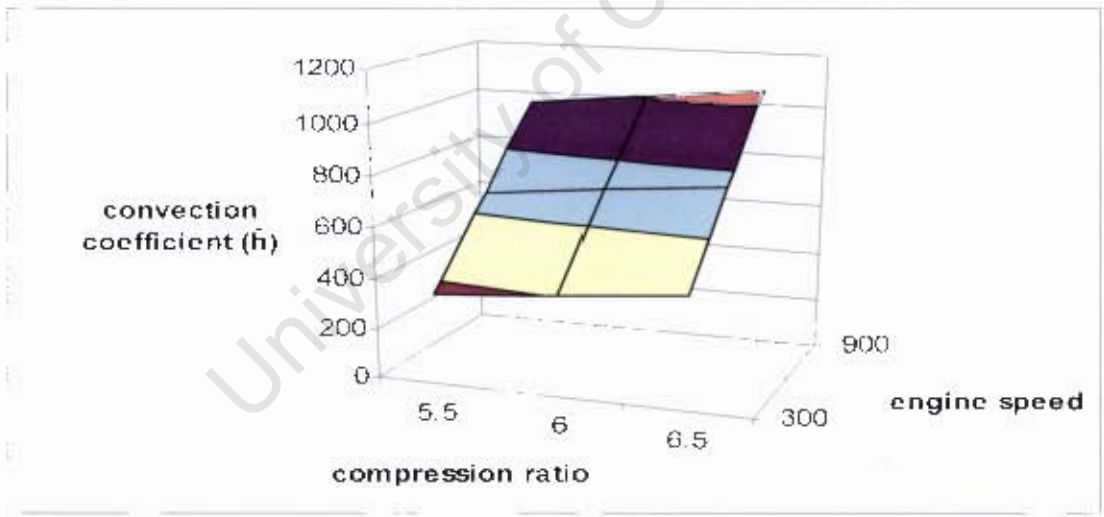

Figure 6-6: Average convection coefficient plotted in relation to engine speed and compression ratio

Equation 6-2

$$\hat{h} = 1.0038N + 89.528CR - 433.95$$

A lumped heat capacity was assumed for the tip of the thermocouple and was used to estimate the gas temperature from the measured thermocouple temperature. The gas temperature was estimated using the temperature at the thermal equilibrium point of the thermocouple and the convection coefficient from Equation 6-2, using Equation 6-3. which includes a function of

engine speed and wall temperature to account for changing boundary layer thicknesses and heat conduction to the walls of the engine.

Equation 6-3

$$\hat{h}A_s(T_g - T) + mC_p\frac{dT}{dt} + f(N, T_w) - 0$$

6.1.1 Predicting the bulk gas temperatures for the motored engine

Calculations done using Equation 6-3 for the motored engine were performed at the CAD of the thermocouple's thermal equilibrium, to determine the trapped cylinder mass and then the gas temperature profile was calculated from the measured pressure assuming the ideal gas law. The temperatures were found to be in good agreement with the estimated calculation of the ideal gas law while estimating the mass. The error range produced from the calculated temperature was ±40°C at the point of calculation, and this could translate to ±70°C at TDC. Examples of some of the calculations are shown below, exhibiting cases of close matches, over-prediction and under-prediction. The inability of the model to estimate the bulk gas temperature with better accuracy stems from the fact that the average convection coefficient in Equation 6-2 is estimated assuming direct proportionality to engine speed and compression ratio, but in reality this was not the case.

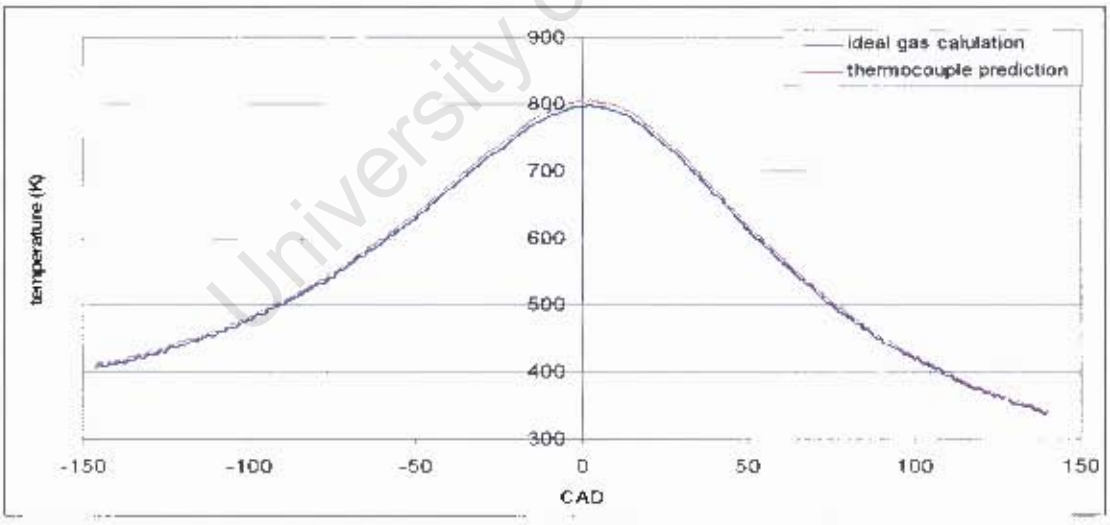

Figure 6-7: Comparison of the temperature predicted using the thermocouple measurement compared to the ideal gas calculation with an estimated mass at 600rpm and compression ratio 5.5.

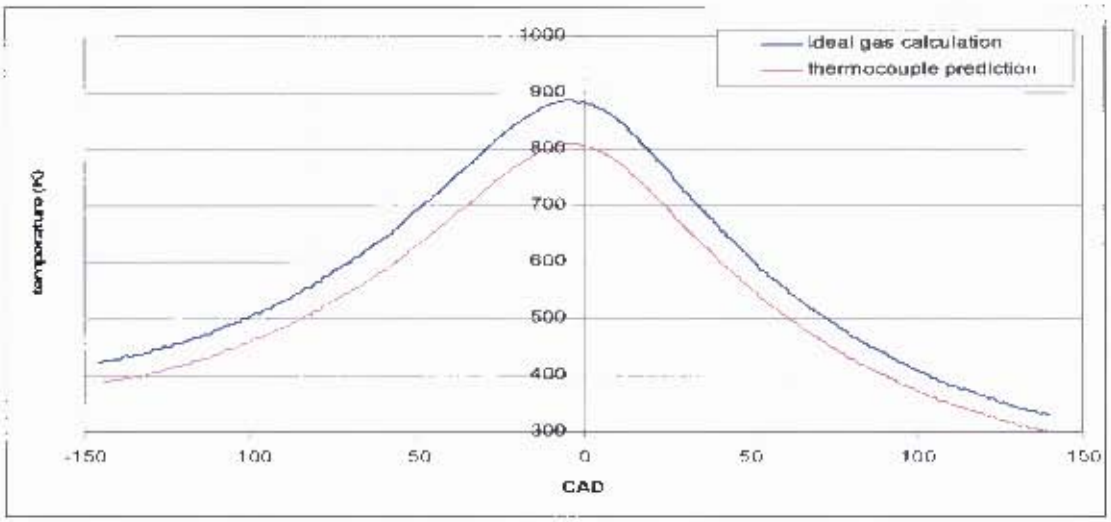

Figure 6-8: Comparison of the temperature predicted using the thermocouple measurement compared to the ideal gas calculation with an estimated mass at 600rpm and compression ratio 7.0.

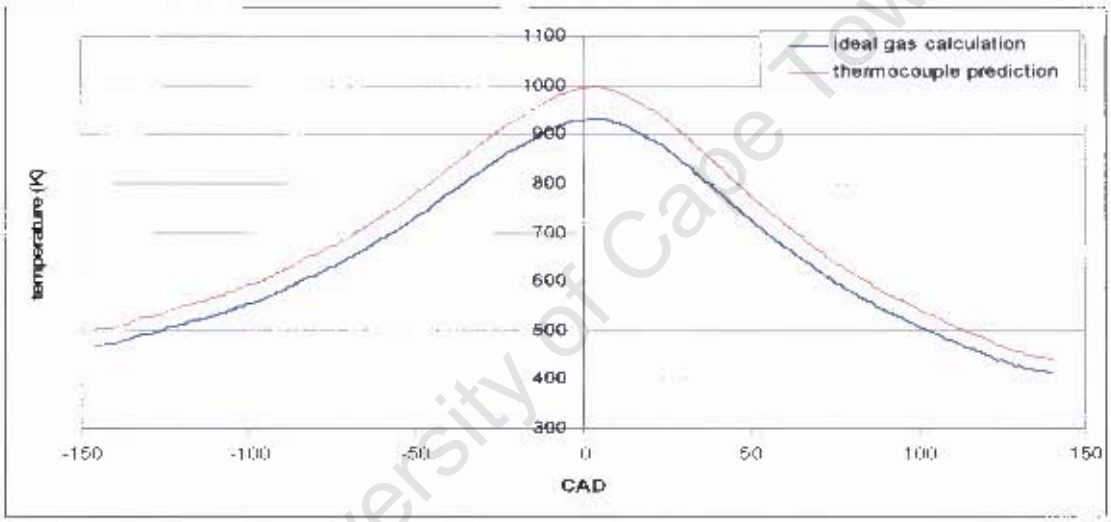

Figure 6-9: Comparison of the temperature predicted using the thermocouple measurement compared to the ideal gas calculation with an estimated mass at 900rpm and compression ratio 5.5.

6.1.2 Predicting the bulk gas temperatures for the fired engine

As mentioned in chapter 3.2.2, Hall and Bracco (1986) stated that gas motion within a cylinder of a fired engine before the onset of combustion is similar to that in a motored engine. With this in mind, Equation 6-3, with similar coefficients to those used to calculate the motoring cycles was used to predict bulk gas temperature in the fired engine.

The calculation appeared to under-predict the bulk gas temperature by as much as 100°C at the CAD of the thermocouple's thermal equilibrium, when compared to simulated temperatures. An example is shown in Figure 6-10. It must be kept in mind however that the simulated temperature profile is sensitive to the temperature at IVC which varied during the experiment

due to cycle-cycle variations. Temperatures during the compression stroke have been shown to vary by as much as 60°C, at the same CAD. (Hajireza et al. 1999)

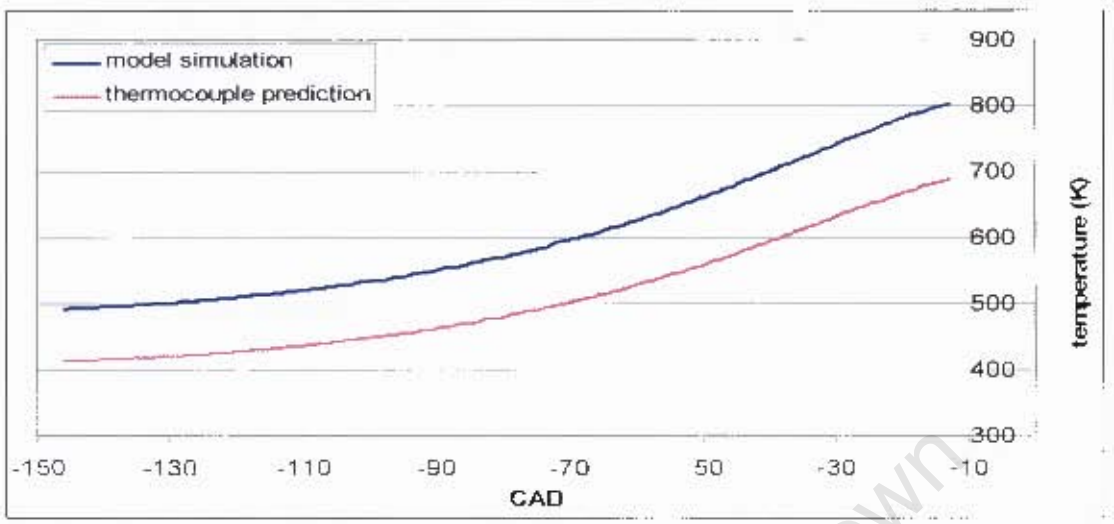

Figure 6-10: Comparison of the temperature predicted using the thermocouple measurement compared to a simulated profile at 600rpm and compression ratio 5.5.

6.2 Effect of the boundary layer on heat transfer to the thermocouple

The effect of the boundary layer was fully incorporated in the heat transfer model used. It was found that the 2mm and the 4mm thermocouple were located within the boundary layer during the motored cycle. Modelling of the temperature profile within the thickness of the boundary layer and the heat transfer to the thermocouple were done using the model described in chapter 3.2.1. Figure 6-11 below shows the typical profile of the boundary layer temperature.

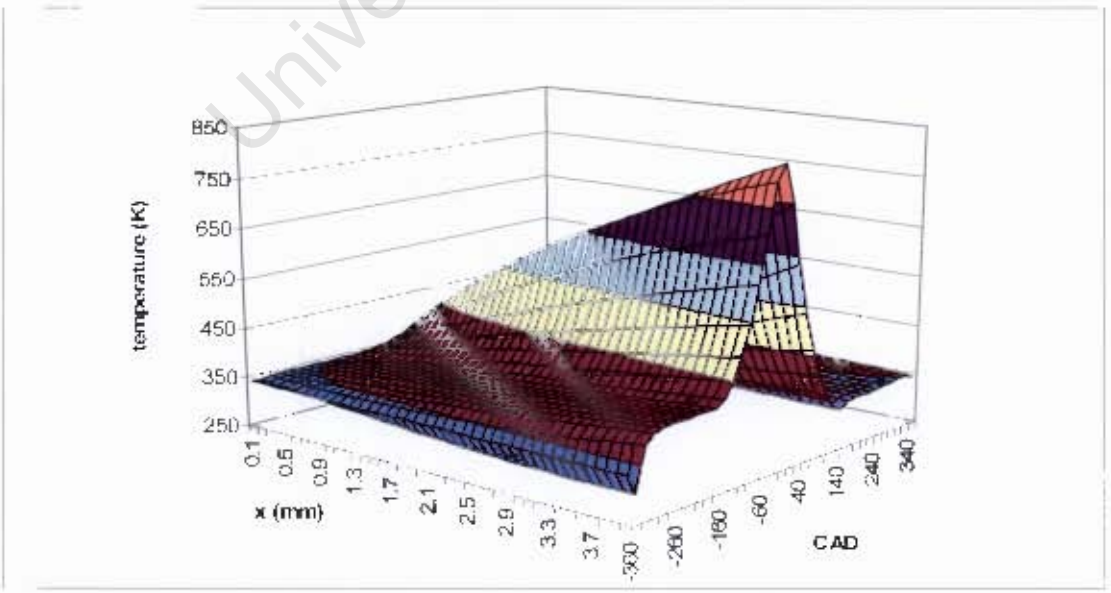

Figure 6-11: Thermal boundary layer profile at 600rpm and compression ratio 6.5.

Figure 6-12 and Figure 6-13 below show the temperature profiles plotted against distance from the cylinder wall at different crank angle degrees for the compression stroke and the expansion stroke. Figure 6-13 shows a distinct cool region near the wall, and a characteristic S-shape of the temperature profile in the early part of the expansion stroke. This phenomenon is expected from the work done by Lawton.

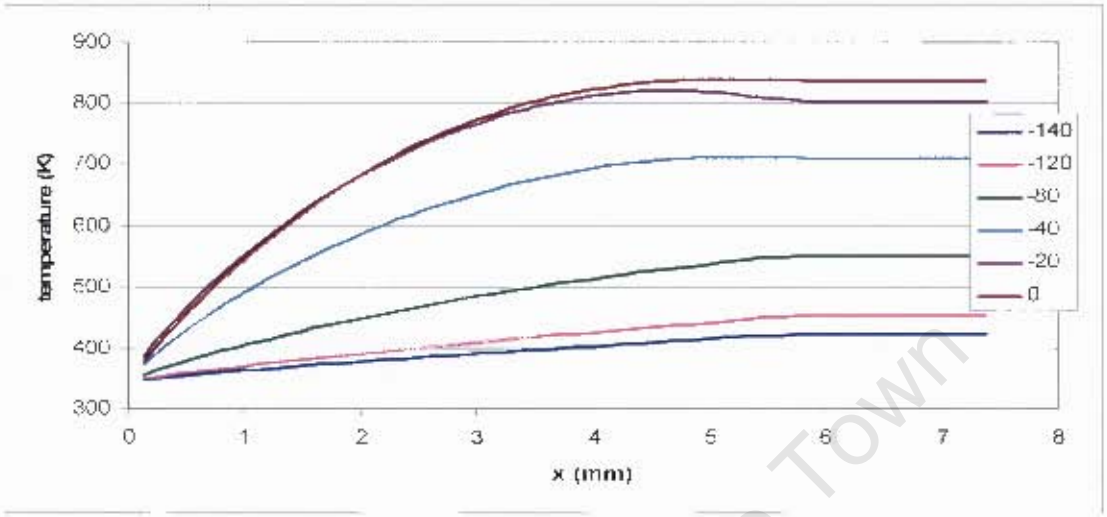

Figure 6-12: Typical boundary layer profile during compression shown at different CAD

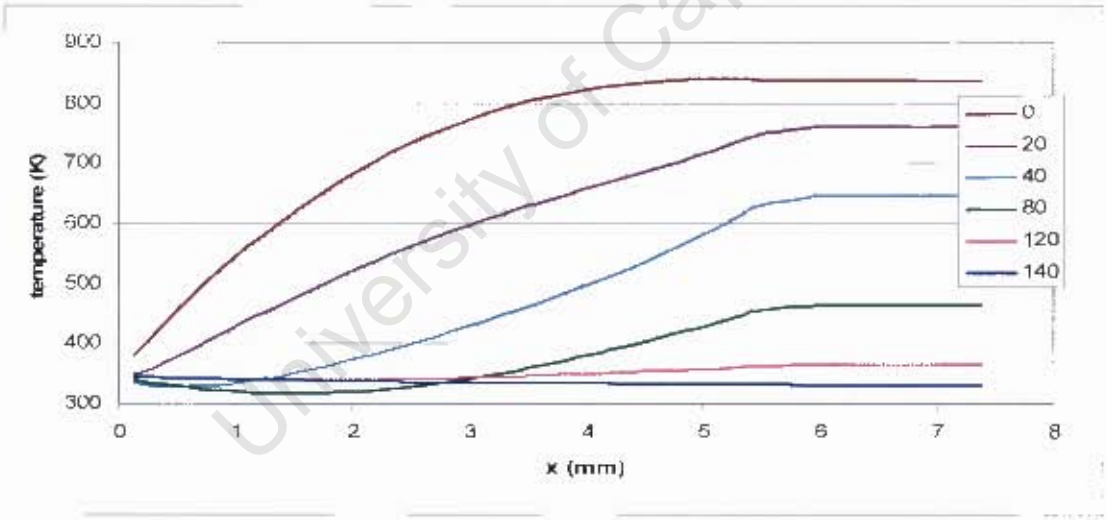

Figure 6-13: Typical boundary layer profile during expansion shown at different CAD

This in effect caused the temperature within the thermocouple to start dropping even though the temperature of the bulk gas was still much higher than the thermocouple temperature.

Figure 5-7 showed that the 4mm thermocouple exhibited a lesser temperature swing than the 2mm thermocouple, and this result was not expected from the onset. But after careful analysis of literature available, Hsiao (2006), who modelled the flow inside the CFR engine showed swirl flow forming a forced vortex during the inlet process and this form for the velocity profile is maintained during compression stroke. Results from Hsiao's work show that the there is a

sharp increase in air velocity from the cylinder wall, which reaches a maximum value in close proximity of the wall, then falls off rapidly towards the centre of the cylinder. This should, in effect, cause a decrease in the convection away from the cylinder walls, thus reducing convection heat transfer to the tip of the longer 4mm thermocouple. Work done by Foster and Witze (1987) showed that the turbulence effects of gas motion decreased away from the wall and this might also have caused less convection with distance increasing away from the walls of the cylinder.

However the model described in chapter 3.2.2 used to predict the velocity profile for this project did not capture this form, and this caused the heat transfer model to over-predict the temperature for the 4mm thermocouple.

7. Conclusions and Recommendations

The conclusions presented here are drawn from the results of the investigation, with focus on the objectives set out at the start of the project.

An engine model was successfully created. The engine model, could describe the breathing strokes, compression, and combustion with acceptable and useful accuracy. The two-zone combustion model used simulated the combustion process effectively. It was however found that during the late part of the expansion stroke, heat loss predicted by the engine model was not sufficient to fully describe actual results.

The boundary layer model used to improve the numerical model exhibited acceptable accuracy when predicting the temperature for the 2mm thermocouple. However it was not sufficient to predict the velocity profile and this caused it to over predict the temperature profile of the 4mm thermocouple without substantial changes to the convection coefficient which would have been technically questionable without experimental data.

A heat transfer model for the thermocouple was also successfully created. The heat transfer model managed to capture the general shape of the temperature profile in the thermocouple, showing sensitivities to changes in in-cylinder gas velocities. Thermo-physical properties of the thermocouple material, such as density were taken as a constant and immune to change due to temperature fluctuations. These assumptions proved to have little effect on the sensitivity of the model.

The thermocouple was successfully constructed and used to infer the gas temperature in the engine. The thermocouple however did not manage to capture the desired bulk gas temperature because the thermocouple was situated within the boundary layer and the associated time constant introduced calculation difficulties and consequent prediction uncertainties

With due correction for the thermal boundary layer thickness and the heat transfer to the walls of the engine, the 2mm thermocouple, was shown to be capable of predicting the bulk gas temperatures and achieved accuracies of ±40°C for the motored engine. This compensation technique did not hold true for the fired test results, when coefficients were maintained, errors in temperature of up to 100°C were achieved.

Although the numerical model used in this project could be further improved to describe the temperature in the thermocouple with more accuracy, it would not enhance the measuring capabilities of the method, since the uncertainties in the transformation to a fired engine would remain.

For the measurement of gas temperature in the combustion engine it is recommended that the research group should explore the possibility of making use of acoustic methods. This is because they are relatively simpler and cheaper than laser based methods. Although acoustic methods have been shown to exhibit uncertainties due to changing conditions in the cylinder; pressure, temperature and gas composition, they have not appeared to have compromised the accuracy greatly when compared to laser based methods when used for bulk gas temperature determination.

8. References

Arpaci, V. S. and Larsen, P. S. (1984), *Convection Heat Transfer*, Prentice-Hall, Inc.

Aust, V., Zimmermann, G., Manz, P. and Hentschel, W. (1999), *Crank-Angle Resolved Temperature in SI Engines Measured by Emission-Absorption Spectroscopy*, SAE 1999-01-3542

Bauer, W., Heywood, J. B., Avanessian O. and Chu D. (1996), *Flow characteristics in intake port of spark ignition engine investigated by CFD and transient gas temperature measurement*, SAE 961997

Bauer, W., Tam C., Heywood, J. B. and Ziegler, C. (1997), *Fast Gas Temperature Measurement by Velocity of Sound for IC Engine Applications*, SAE 972826

Bood, J., Bengtsson, P., Mauss, F., Burgdorf, K. and Denbratt, I. (1997), *Knock in Spark Ignition Engines: End-Gas Temperature Measurements Using Rotational CARS and Detailed Kinetic Calculations of the Autoignition Process*, SAE 971669

Cengel, Y. A. and Boles, M. A. (2002), *Thermodynamics: An engineering approach*, fourth edition, McGraw-Hill Book Company

Cessac, K. J. (2003), *Reducing Thermowell Conduction Errors in Gas Pipeline Temperature Measurement*, AIP Conference Proceedings, Volume 684, Issue 1, Pages 1093-1096

Enomoto, Y., Nagano, H., Hagihara, Y. and Koyama, T. (1997), *Thermal load in D.I diesel engine under EGR operation-measurements of steady state temperature of combustion chamber wall surface and intake gas temperature*, JSAE 0733594

Fiveland, S. B. and Assanis, D. N. (2001), *Development of a Two-zone HCCI Combustion Model Accounting for Boundary Layer Effects*, SAE 2001-01-1028

Foster, D. E. and Witze, P. O. (1987), *Velocity Measurements in the Wall Boundary Layer of a Spark-Ignited Research Engine*, SAE 872105

Hajireza, S., Sunden, B. and Mauss, F. (1999), *A Three-Zone Model for Investigation of Gas Behaviour in the Combustion Chamber of SI Engines in Relation to Knock*, SAE 1999-01-0219

Hall, M. J. and Bracco, F. V. (1986), *Cycle-Resolved Velocity and Turbulence Measurements near the Cylinder Wall of a Firing S.I Engine*, SAE 861530

Heywood, J. B. (1988), *Internal Combustion Engine Fundamentals*, McGraw-Hill Book Company

Holman, J. P. (2002), *Heat Transfer, Ninth Edition*, McGraw-Hill Book Company

Hsiao, T. (2006), Master's Thesis, *Flame Propagation Model for the CFR Engine under Knocking and Non-Knocking Conditions*, University of Cape Town (Unpublished)

Ishii, A., Nagano, H., Kimura, S., Koike, M., Iida, N., Ishii, H. and Enomoto, Y. (2000), *Measurement of Instantaneous Heat Flux Flowing Into Metallic and Ceramic Combustion Chamber Walls*, SAE 2000-01-1815

Jenkin, R. J., James, E. H. and Malalasekera, W. (1996a), *Modelling Near Wall Temperature Gradients in "Motored" Spark Ignition Engines*, SAE 960070

Jenkin, R. J., James, E. H. and Malalasekera, W. (1996b), *Thermal Boundary Layer Modelling in 'Motored' Spark Ignition Engines*, SAE 961965

Kar, K. Roberts, S., Stone, R., Oldfield, M. and French, B. (2004), *Instantaneous Exhaust Temperature Measurements Using Thermocouple Compensation Techniques*, SAE 2004-01-1418

Kawahara, N., Tomita, E. and Kamakura, H. (2001), *Transient temperature measurement of gas using Fiber Optic Heterodyne Interferometry*, SAE 2001-01-1922

Lawton, B. (1987), *Effect of compression and expansion on instantaneous heat transfer in reciprocating internal combustion engines*, Proceedings of the Institute of Mechanical Engineers, Volume 201, Number A3, Pages 175-186.

Lucht, R. P., Walter, T., Dunn-Rankin, D., Dreier, T. and Bopp, S. C. (1991), *Heat Transfer in Engines: Comparison of Cars Thermal Boundary Layer Measurements and Heat Flux Measurements*, SAE 910722

Lyford-Pike, E. J. and Heywood, J. B. (1984), *Thermal boundary layer thickness in the cylinder of a spark-ignition engine, International Journal of Heat and Mass Transfer*, Volume 27, Number 10, Pages 1873-1878.

Sanders, S. T., Kim, T. and Ghandhi, J. B. (2003), *Gas Temperature Measurement during Ignition in an HCCI Engine*, SAE 2003-01-0744

Sanderson, S. R. and Sturtevant, B. (2002), *Transient heat flux measurements using a surface junction thermocouple*, Review of Scientific Instruments, Volume 73, Number 7, Pages 2781-2787

Sundqvist, B. (1992), *Thermal diffusivity and thermal conductivity of Chromel, Alumel, and Constantan in the range 100K-450K*, Journal of Applied Physics, Volume 72, Issue 2, Pages 539-545

APPENDICES

A. Numerical model development

A.1 Combustion model

A two-zone model was used to simulate combustion pressures and temperatures. Conditions at IVC are set from the end conditions at the end of the breathing cycle calculation and the fuel type and air/fuel ratio are manually defined. The pressure was solved by maintaining an energy balance before the spark was initiated. After the spark had been initiated the mass fraction of the charge burned was calculated using the Wiebe function, the burned volume calculated and the pressure and burned temperatures solved, while maintaining an overall energy balance. Gas species were also solved for simultaneously to maintain a chemical equilibrium. The calculation ended once EVO was reached. Shown in Figure A-1 is a flow diagram of the engine model from IVC to EVO.

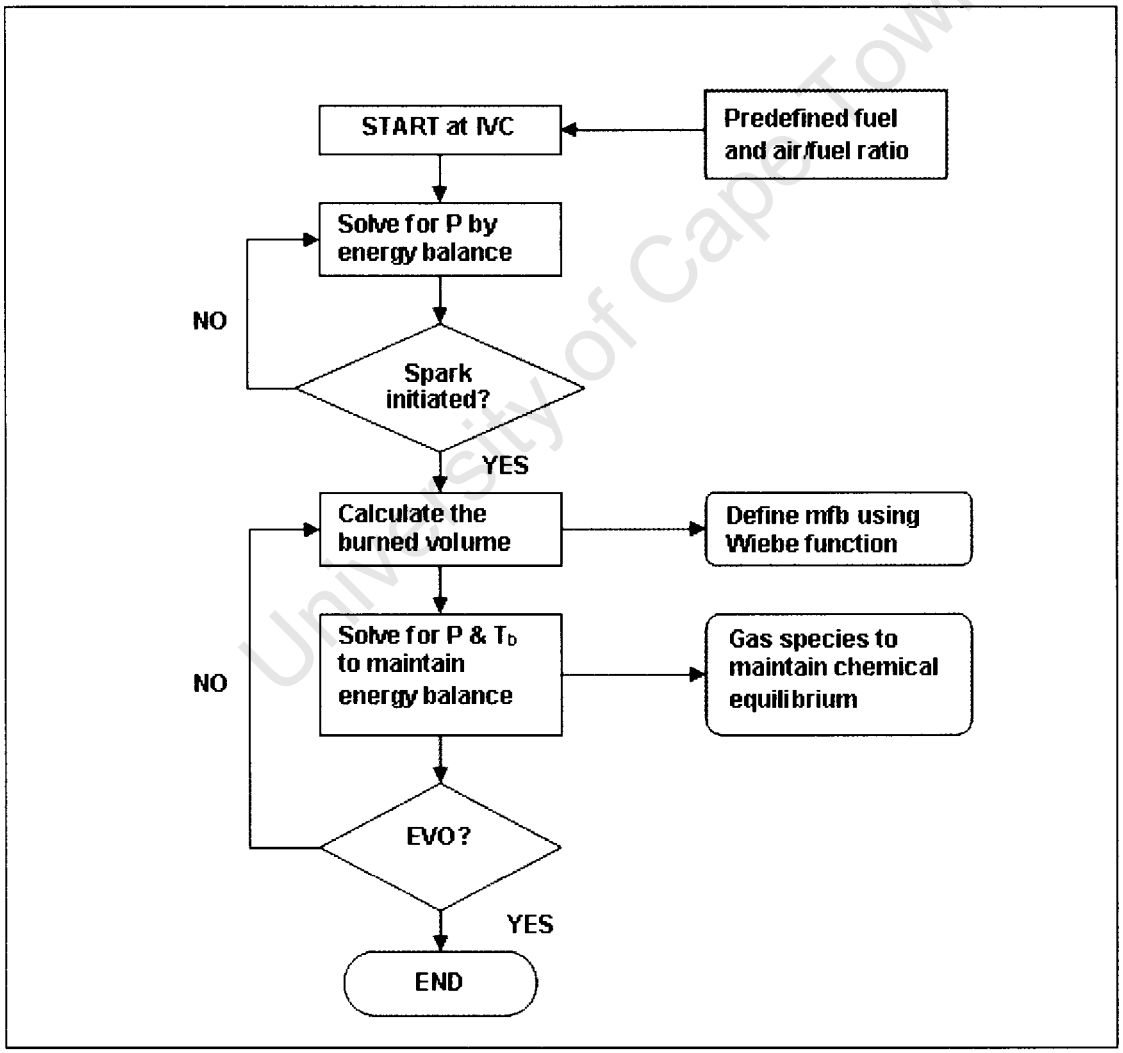

Figure A-1: Flow diagram for the combustion model

At the end of the combustion model are imported to be starting conditions for the engine breathing model.

A.2 Engine breathing model

At the start of the exhaust process the cylinder pressure and temperature were defined from the conditions at EVO, and thereafter they were defined by the following equations.

The temperature within the cylinder at any point in time was assumed to follow the ideal gas law.

Equation A-1

$$T_{cyl} = \frac{PV}{mR}$$

The mass at every step through the iteration was defined by Equation A-2, and the density also obeyed the ideal gas law.

Equation A-2

$$m_2 = m_1 + \Delta m$$

Equation A-3

$$\rho_{cyl} = \frac{P}{RT}$$

The velocity of the gas through the valves was governed by the difference in pressure between the cylinder and the manifold using Bernoulli's equation and assuming incompressible flow. The direction of gas flow was determined by the comparison of the cylinder pressure to the manifold pressure.

Equation A-4

$$v_v = \sqrt{2\left|P_{cyl} - P_{man}\right| / \rho}$$

And ρ is either ρ_{man} or ρ_{cyl}, determined by the direction of fluid flow.

Equation A-5

$$\Delta m = \dot{m}\Delta t$$

Where $\dot{m} = \rho A v_v$ and ρ is determined by the direction of fluid flow

The effective area through the valve is then the product of the curtain area available when the valve opens and the discharge coefficient, determined by the geometry.

Equation A-6

$$A = A_v \cdot C_D$$

During the intake process, losses through the intake manifold are calculated as follows:

Based on Δm, the velocity through the inlet manifold can be calculated from the following equation.

Equation A-7

$$v_{man} = \frac{\Delta m / \Delta t}{\rho_{man} \cdot A_{man}}$$

Equation A-8

$$P_{man} = P_{amb} - \Delta P_{man}$$

Where ΔP_{man} is a combination of the losses encountered at the manifold entry and the through the elbows, and the losses as a result of friction through the manifold.

Equation A-9

$$\Delta P_{man} = \tfrac{1}{2} K_{in} \rho v^2 + \frac{4FL}{D} \cdot \frac{\rho v^2}{2}$$

$$\Delta P_{man} = \left(K_{in} + \frac{4FL}{D} \right) \cdot \tfrac{1}{2} \rho_{man} v_{man}^2$$

Changes in the enthalpy, work done and internal energy are shown in Equation A-10 to Equation A-12.

Equation A-10

$$\Delta h = \Delta m \cdot C_p \cdot T$$

Where T is chosen appropriately as either manifold or cylinder temperature

Equation A-11

$$\Delta W = \frac{1}{2}(P_1 + P_2) \cdot (V_2 - V_1)$$

Equation A-12

$$U_{cyl} = m_2 \cdot C_v \cdot T_{cyl}$$

A cylinder pressure is calculated to maintain the overall energy balance in Equation A-13.

Equation A-13

$$U_2 - U_1 + \Delta W - \Delta Q - \Delta h = 0$$

A.3 Numerical solution to thermal energy equation

Numerical solution to equation 3-9, has been provided by Lawton (1987). The equation has been solved by a simple explicit finite difference scheme as follows:

Equation A-14

$$\frac{\partial T}{\partial t} = \frac{G_i - T_i}{\delta t}$$

Equation A-15

$$\frac{\partial T}{\partial x} = \frac{T_{i+1} - T_{i-1}}{2\delta x}$$

Equation A-16

$$\frac{\partial^2 T}{\partial x^2} = \frac{T_{i-1} - 2T_i + T_{i+1}}{\delta x^2}$$

Substituting Equation A-14 to Equation A-16 into equation 3-9 gives

Equation A-17

$$G_i = (1 - 2p_i - u)T_i + p_i(T_{i-1} + T_{i+1})$$

Where

$$p_i = \alpha_i \frac{\delta t}{\delta x^2}$$

And

$$u = \frac{\gamma - 1}{V}\frac{dV}{dt}\delta t$$

B. Thermo-physical properties for k-type thermocouple

Table B-1 and Table B-2 provide the thermo-physical properties for Alumel and Chromel, used in this project, from work by Sundqvist (1992).

Table B-1: Thermo-physical properties for Alumel

T (K)	α (mm^2/s)	C_p (J/kg/K)	k (W/m/K)
275	7.36	452	28.5
300	7.34	464	29.2
325	7.32	476	29.9
350	7.30	489	30.6
375	7.25	501	31.1
400	7.16	515	31.6
425	7.14	510	31.9
450	7.53	502	32.6

The paper however did not provide specific heat values (C_p) for Chromel, thus Equation B-1 was used to calculate the C_p values.

Equation B-1

$$C_p = \frac{k}{\alpha\rho}$$

Table B-2: Thermo-physical properties for Chromel

T (K)	α (mm^2/s)	k (W/m/K)
275	4.63	16.7
300	4.68	17.3
325	4.75	17.8
350	4.82	18.4
375	4.91	19.0
400	5.00	19.7
425	5.09	20.3
450	5.19	21.0

C. Results

The following figures show the comparison of the bulk gas temperature as predicted using the ideal gas equation and the gas temperature inferred from the 2mm thermocouple readings.

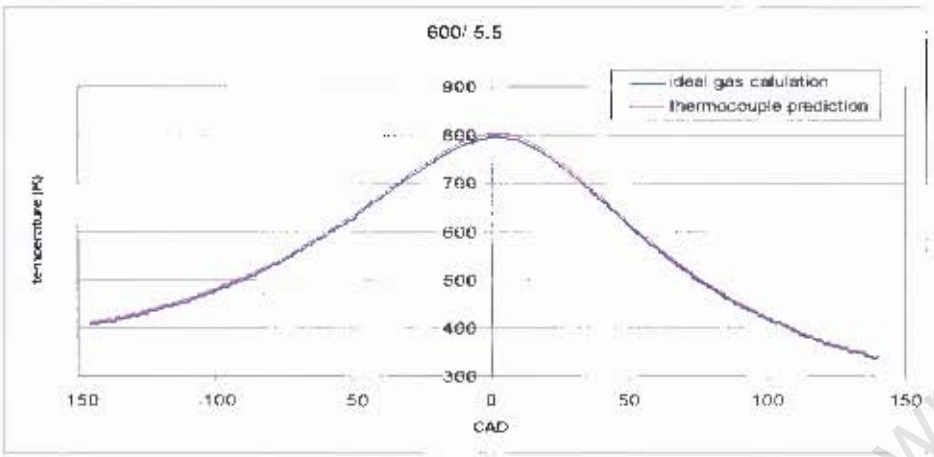

Figure C-1: Comparison of the temperature predicted from the thermocouple measurement compared to the ideal gas calculation at 600rpm and compression ratio 5.5.

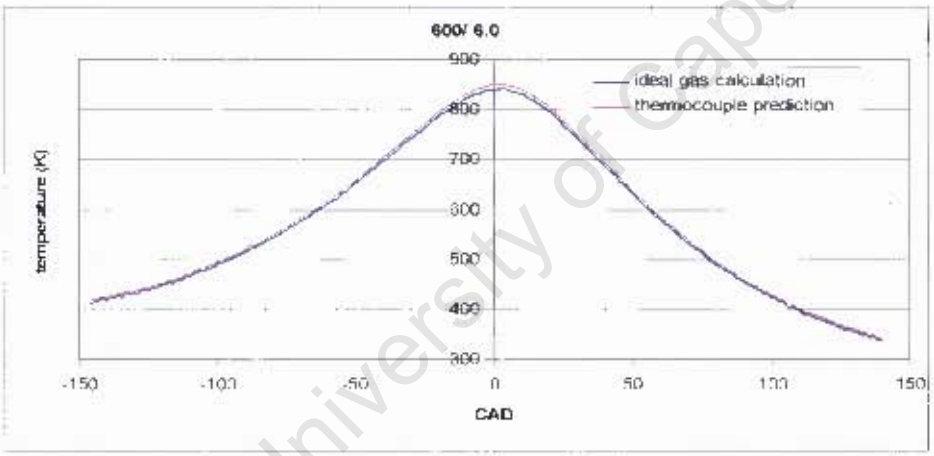

Figure C-2: Comparison of the temperature predicted from the thermocouple measurement compared to the ideal gas calculation at 600rpm and compression ratio 6.0.

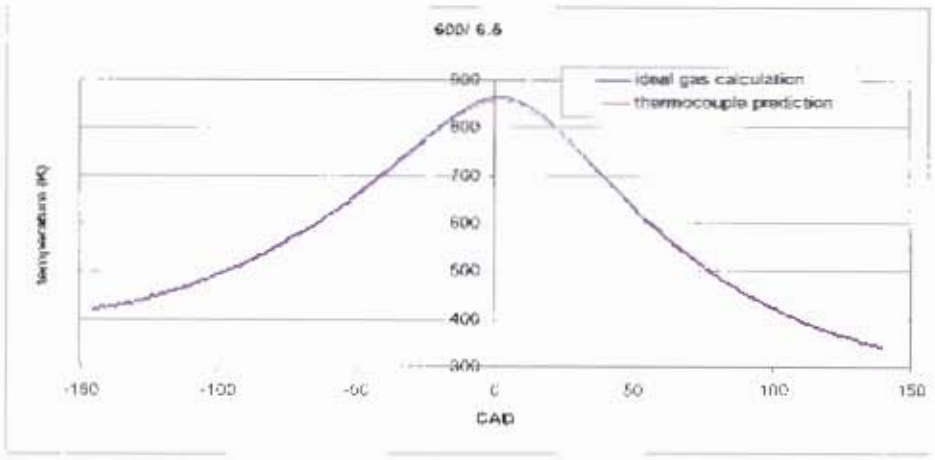

Figure C-3: Comparison of the temperature predicted from the thermocouple measurement compared to the ideal gas calculation at 600rpm and compression ratio 6.5.

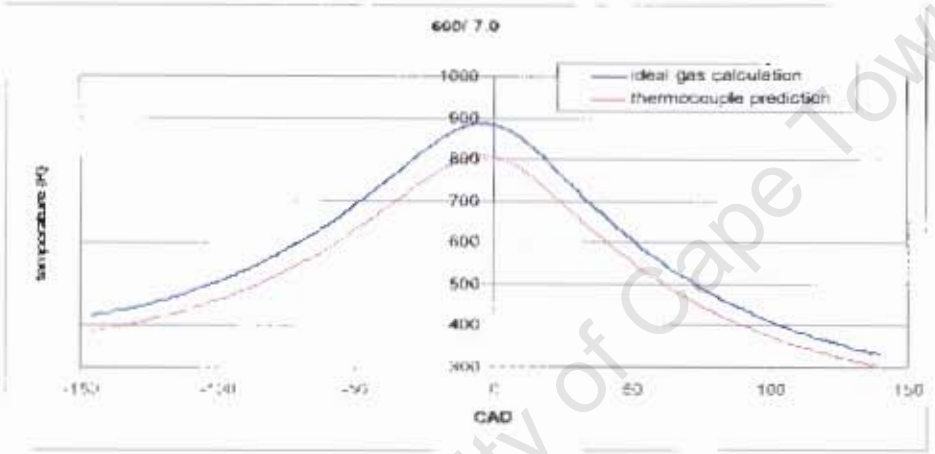

Figure C-4: Comparison of the temperature predicted from the thermocouple measurement compared to the ideal gas calculation at 600rpm and compression ratio 7.0.

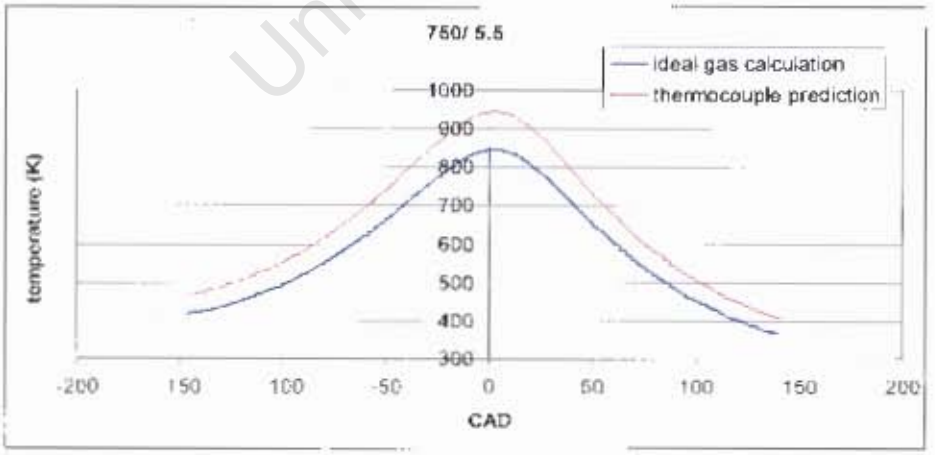

Figure C-5: Comparison of the temperature predicted using the thermocouple measurement compared to the ideal gas calculation at 750rpm and compression ratio 5.5.

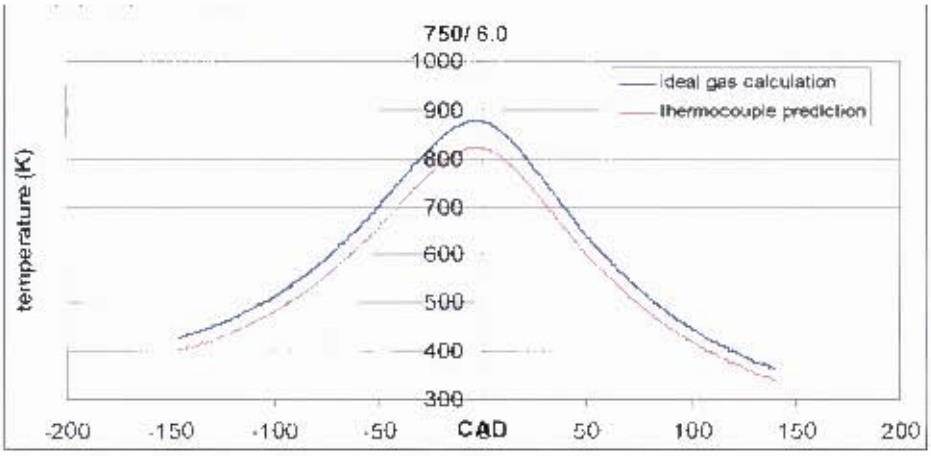

Figure C-6: Comparison of the temperature predicted from the thermocouple measurement compared to the ideal gas calculation at 750rpm and compression ratio 6.0.

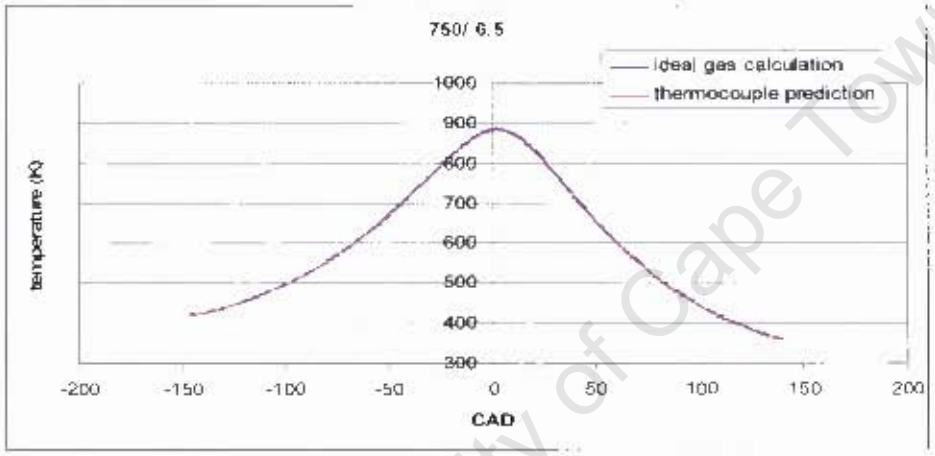

Figure C-7: Comparison of the temperature predicted from the thermocouple measurement compared to the ideal gas calculation at 750rpm and compression ratio 6.5.

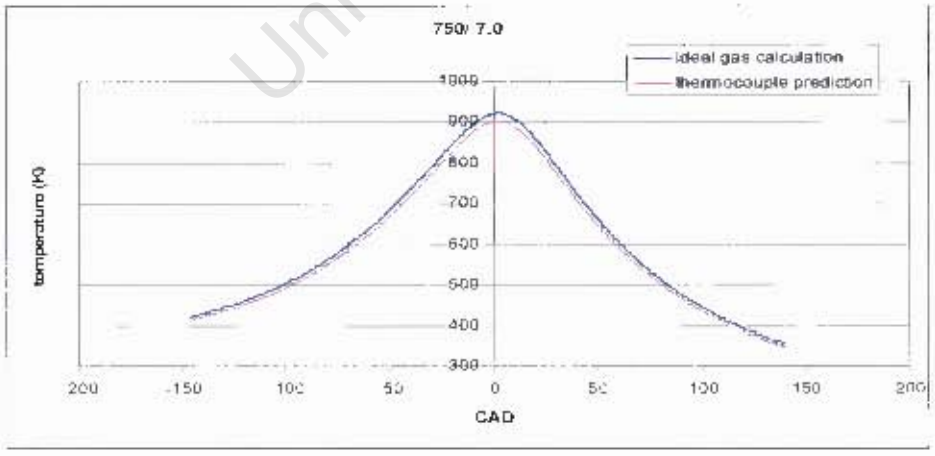

Figure C-8: Comparison of the temperature predicted from the thermocouple measurement compared to the ideal gas calculation at 750rpm and compression ratio 7.0.

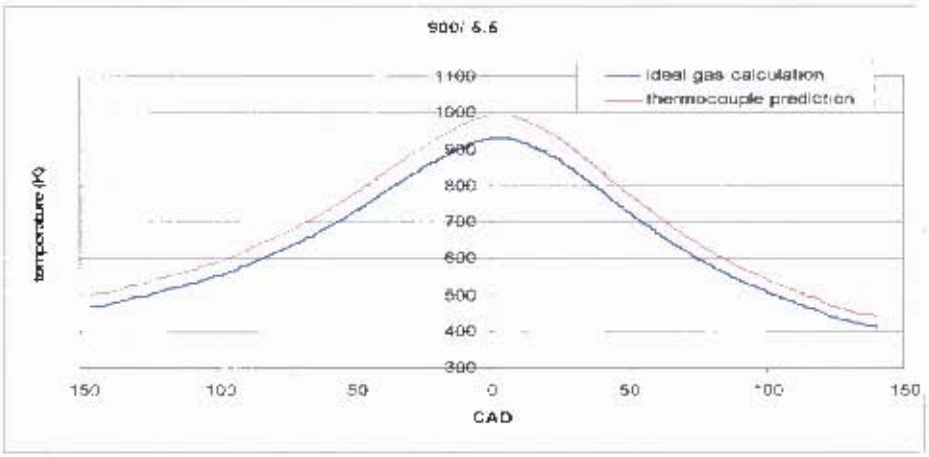

Figure C-9: Comparison of the temperature predicted from the thermocouple measurement compared to the ideal gas calculation at 900rpm and compression ratio 5.5.

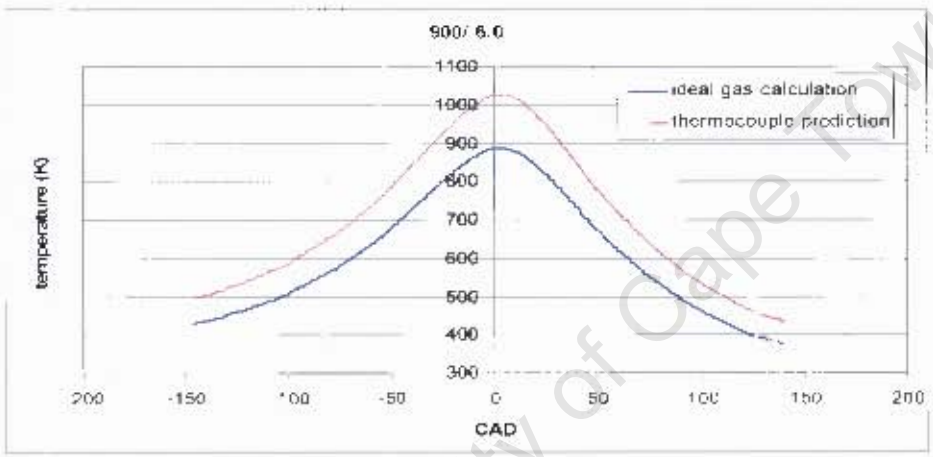

Figure C-10: Comparison of the temperature predicted from the thermocouple measurement compared to the ideal gas calculation at 900rpm and compression ratio 6.0.

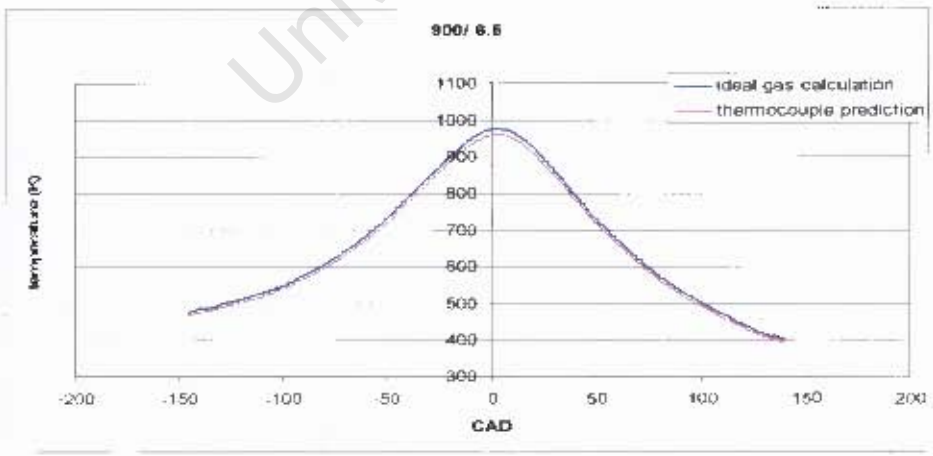

Figure C-11: Comparison of the temperature predicted from the thermocouple measurement compared to the ideal gas calculation at 900rpm and compression ratio 6.5.

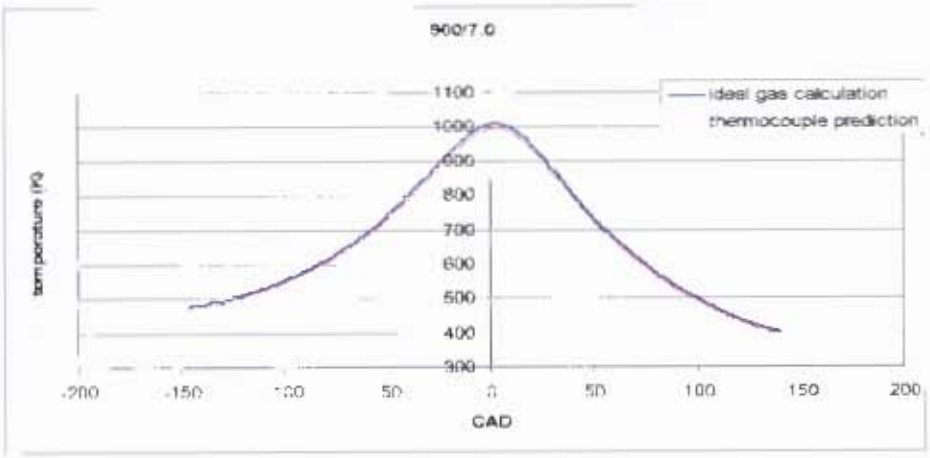

Figure C-12: Comparison of the temperature predicted from the thermocouple measurement compared to the ideal gas calculation at 900rpm and compression ratio 7.0.